A DISSERTATION ON

Physico-Chemical Characterization of Lithium-Rich Metal Oxides: $Li_{1+x}M_{1-x}O_2$ [M=Mn, Ni, Fe and x=0.2] Cathode Material for Lithium-Ion Batteries

Submitted in partial fulfilment of

the requirement for the award of the degree of

MASTER OF TECHNOLOGY

In

NANOSCIENCE AND TECHNOLOGY

Submitted By

RISHIBRIND KUMAR UPADHYAY

(2K12/NST/18)

Under the Supervision of

DR. AMRISH K. PANWAR

DEPARTMENT OF APPLIED PHYSICS

DELHI TECHNOLOGICAL UNIVERSITY

(FORMERLY DELHI COLLEGE OF ENGINEERING)

NEW DELHI-110042

July 2014

DEDICATION

This thesis is dedicated to my parents.

CERTIFICATE

This is to certify that the thesis entitled **"Physico-Chemical Characterization of Lithium-Rich Metal Oxides: $Li_{1+x}M_{1-x}O_2$ [M=Mn, Ni, Fe and x=0.2] Cathode Material for Lithium-Ion Batteries"**, submitted by **Rishibrind Kumar Upadhyay (2K12/NST/18)** in partial fulfillment of the requirements for the award of the degree of Master of Technology in Nanoscience and Technology is carried out at Lithium-Ion Battery Technology Laboratory, Department of Applied Physics, Delhi Technological University (Formerly Delhi College of Engineering), is an authentic record of the candidate's own work carried out by him under my guidance.

The information and data enclosed in this dissertation is original and has not been submitted to any University/Institute for the award of any other degree.

Date:

Dr. Amrish K. Panwar	**Prof. S. C. Sharma**
Project Supervisor	Head of Department
Department of Applied Physics	Department of Applied Physics
Delhi Technological University	Delhi Technological University

DECLARATION

I hereby declare that the work presented in this thesis entitled **"Physico-Chemical Characterization of Lithium-Rich Metal oxides: $Li_{1+x}M_{1-x}O_2$ [M=Mn, Ni, Fe and x=0.2] Cathode Material for Lithium Ion Batteries"**, has been carried out by me under the guidance of **Dr. Amrish Kumar Panwar** Assistant Professor and hereby submitted for the partial fulfillment for the award of degree of Master of Technology in Nanoscience and Technology at Applied Physics Department, Delhi Technological University (Formerly Delhi College of Engineering), New Delhi.

I further undertake that information and data enclosed in this dissertation is original and has not been submitted to any University/Institute for the award of any other degree.

Date:

Rishibrind Kumar Upadhyay

2K12/NST/18

M.Tech, Nano Science and Technology

Department of Applied Physics

Delhi Technological University

ACKNOWLEDGEMENTS

In pursuit of this academic endeavour, I feel that I have been especially fortunate as inspiration, guidance, direction, co-operation, love and care all came in my way in abundance and it seems almost an impossible task for me to acknowledge the same in adequate terms.

With deep sense of gratitude, I wish to express my sincere thanks to my guide **Dr. Amrish K. Panwar** for giving me the opportunity to conduct Alternative Cathode material of Lithium Ion Battery research and their constant and selfless support at every stage of my project work in Lithium Ion Battery Technology Lab, Applied Physics Department, Delhi Technological University (Formerly Delhi College Of Engineering), New Delhi. Without their guidance and advice this dissertation would not be what it is today. Their patience and support rescued me from despair on countless occasions.

I express my deep appreciation and gratitude to **Prof. S. C. Sharma** and **Dr. Pawan Kumar Tyagi** Department of Applied Physics, Delhi Technological University (Formerly Delhi College of Engineering), New Delhi, for his excellent guidance and support throughout the work. I received very useful and excellent academic training from him, which has stood in good stead while writing this thesis. His unique inimitable style has left an indelible impression on me. His constant encouragement, help and review of the entire work during the course of the entire project.

I am also appreciated the help of Mr. Sandeep Mishra for Characterization in Advanced Instrumentation Center (AIC) at Delhi Technological University (Formerly Delhi College of Engineering), New Delhi.

I am sincerely thankful to the members of my research group Mr. Rakesh Saroha, Mr. Aditya Jain for their continuous support, helpful discussions and assistance.

My sincere thanks to all my batch mates and beloved friends for their encouragement and kind help extended toward me.

Last, but certainly not least, this work is dedicated to my parents. I owe everything of this research work sincerely to their care and affection, without which all this would just have been a dream.

TABLE OF CONTENTS

LIST OF FIGURES

LIST OF TABLES

LIST OF ABBREVIATIONS

Abbreviation	Full name
LIB	Lithium-Ion Battery
Li	Lithium
SEM	Scanning electron microscopy
Ni	Nickel
Fe	Iron
Mn	Manganese
C-rate	Current rate
XRD	X-ray Diffraction
A.U	Arbitrary Unit
Eq.	Equation
EDS	Energy dispersive spectroscopy
EVs	Electric vehicles
HEVs	Hybrid electric vehicles
MCMB	mesocarbon microbeads
JCPDS	Joint committee on powder diffraction standards
EC/DMC	ethylene carbonate/dimethyl carbonate

LIST OF PUBLICATION

[1]. **Rishibrind K. Upadhyay**, Amrish K. Panwar, "Physico-Chemical Characterization of Cathode Material $Li_{1+x}\{Mn_{0.4}Ni_{0.4}Fe_{0.2}\}_{1-x}O_2$ (x=0.2) for Lithium Ion Batteries", *International Journal of Emerging Technology and Advanced Engineering*, **2014**, *4*, 249-253.

ABSTRACT

A cathode material is key factor influencing the high power and high efficiency performances of lithium-ion batteries. The present work attributes to finding a alternative cathode material which would have high cell voltage, high life cycle, high specific energy, safety and cost effective. So a new cathode material of layered structure, were successfully synthesized by sol-gel route. The AC conductivity performance in lithium-ion batteries was also measured by LCR Meter.

The alternative cathode materials as ordinate of well establish layered cathode material, $LiCoO_2$ are enormously in demand for lithium ion batteries due to the costly of Co based cathode at high temperature (>90^0C), toxicity and high cost. $LiMnO_2$, with its higher theoretical capacity (280 $mAhg^{-1}$), lower price and environmental friendliness seems to be an attractive alternative cathode material for Lithium-ion Batteries. This material, however, is structurally unstable, which implies insufficient cyclability of Manganese oxide based batteries. There have been numerous attempts to improve its structural stability. Addition of extra lithium will tend to push the manganese away from trivalent to tetravalent, thus minimizing the impact of any Jahn-Teller distortion coming from Mn^{3+}.

In the present investigation, synthesis of alternative Lithium-Rich Metal oxides $Li_{1+x}M_{1-x}O_2$ [M=Mn, Ni, Fe and x=0.2] cathode material in air & inert atmosphere has been carried out by sol-gel route of chemical synthesis using citric acid as chelating agent.

It is found that by manganese substitution with nickel and iron improve the structural stability. Hence, nickel and Iron doped $Li_{1+x}Mn_{1-x}O_2$ (x=0.2) having general formula $Li_{1+x}\{Mn_{0.4}Ni_{0.4}Fe_{0.2}\}_{1-x}O_2$ (x=0.2) has the potential to fulfil the above criteria to become a better ordinate of alternative cathode material. The ccomposite exhibit the excellent electrical performance with enhanced AC conductivity. The improved performance was attributed to its well ordered layered structure and small particles with uniform size distribution. The proposal layered materials containing iron may a low cost and eco-friendly energy source materials for large scale Lithium-Ion batteries application However, the electrochemical performance of the above synthesized cathode material yet to be performed to see the real capacity of cathode material.

The proper phase confirmation of $Li_{1+x}M_{1-x}O_2$ (x=0.2) and substituted with Ni and Fe has been confirmed by XRD and uniformly distributed prismatic shape of particle size is observed by SEM.

Keywords: cathode materials, cobalt free cathode, layered oxides, ordinate of $LiCoO_2$, sol-gel route

CHAPTER-1: INTRODUCTION

1.1: Background and Motivation

In the beginning of the 21st century hydrocarbons combustion remains the popular energy source for transportation, but the rate of global warming and projected limits in oil supply require a sustainable alternative of hydrocarbons combustion. Electrochemical storage devices such as Batteries and Super Capacitors and energy conversion devices such as fuel cells show an array of devices alternative to the combustion engine. Presently Battery technology has found very high commercial utility in the form of electric and hybrid electric vehicles (EV/HEV). Lithium-ion (Li-ion) battery technology offers the largest development potential for advanced energy storage of clean electricity and electric vehicles but improving power density is desired for high power applications.[1] due to the higher power its permits shorter charging times that is a very essential aspect for those considering a switch from a combustion-powered vehicle to an EV. Due to the increased power density will decrease Lithium-ion battery charging time. Specific power is defined as the product of voltage and specific current. It can be increased by selecting positive and negative materials which lead to a high voltage and also by increasing overall charge/discharge rates. Replacing the conventional micro-particles of the positive electrode material with nano-particles significantly increases the Electrode/electrolyte interface area which improves overall charge/discharge rates.[2] Accordingly investments for the exploitation of renewable energy resources are increasing worldwide with particular attention to solar, wind and battery power systems. There are many advantages of Batteries Technology as an alternative source of energy storage mechanism. Currently the conventional battery technologies such as lead-acid and nickel cadmium are slowly being replaced by lithium-ion (Li-ion) batteries and fuel-cell technologies. Lithium-ion battery technology stands as a forerunner and market leader when compared to the other possible energy systems.

The main motivation for using this Lithium-ion battery technology is for lightest and most electropositive metallic element, which facilitates very high energy density.[3] Li-ion batteries have been found to be stable over 500 cycles, can be fabricated in different sizes and also require very little maintenance compared to the others. Researchers continue to work on many different aspects of this technology such as decreasing the cost, increasing the cycling life and the safety. This technology is already being used in high-end electronics has recently been introduced to the power tool markets and is entering the hybrid electric-vehicle market making it a serious contender to power the electric motorcars of the future. Despite the promise of higher power density, use of

nano-particles as active material in Li-Ion batteries has not been fully engineered for the electrodes and the nature of electrochemical energy storage is not completely understood. Widespread commercial use of nano-particles in energy devices will require more sophisticated electrode formulations and a better understanding of the nature of charge storage. Therefore this work is motivated by a need for a deeper understanding of nano-particles for use as active material in Li-ion batteries.

1.2: Aim of the Thesis

The aim of this thesis is to synthesize alternative lithium rich cathode material comprised of lithium and other elements that can exhibit high capacities and possibly replace conventional $licoo_2$ cathode material which are effective but are also expensive, toxic & unsafe at high temperature.

1.3: Organization of Thesis

The thesis is divided in five chapter and references.

Chapter 1: is the introduction part. It describes background and motivation, aim of the thesis and organization of thesis.

Chapter 2: presents the literature review, which includes the description of the history of lithium-ion batteries, basic concepts and principles for lithium-ion batteries, selection criteria for lithium-ion batteries systems, nanostructure electrode materials for lithium-ion batteries, nanostructure cathode materials, nanostructure layered oxides, synthesis of $Li_{1+x}M_{1-x}O_2$ [M=Mn, Ni, Fe and x=0.2) and optimization of $Li_{1+x}M_{1-x}O_2$ [M=Mn, Ni, Fe and x=0.2].

Chapter 3: presents the synthesis and characterization, which includes the description of the synthesis of $Li_{1+x}Mn_{1-x}O_2$ (x=0.2), and $Li_{1+x}\{Mn_{0.4}Ni_{0.4}Fe_{0.2}\}_{1-x}O_2$ (x=0.2), experimental setup and characterization techniques.

Chapter 4: related to the Result & Discussion which includes the analysis of $Li_{1+x}Mn_{1-x}O_2$ (x=0.2) and analysis of $Li_{1+x}\{Mn_{0.4}Ni_{0.4}Fe_{0.2}\}_{1-x}O_2$ (x=0.2) in air and inert atmosphere.

Chapter 5: contain conclusion and summary of the work.

CHAPTER-2: LITERATURE REVIEW

Due to the high energy density and high power density Lithium-ion batteries have proved themselves the most advanced electrochemical power sources for portable electronic devices in the past two decades. Recently lithium-ion batteries have made a great impact on vehicle electrification, electric vehicles (EVs) and including hybrid electric vehicles (HEVs) in response to the concern to reduce air pollution and global warming.[4-7] However, the current generation of lithium-ion batteries cannot meet the stringent requirements of high power application in terms of cycle life, energy density, power density, cost, safety and environmental concerns.[8] Great efforts have been devoted to increasing the electrochemical performance of lithium-Ion battery systems by using nanoscience and Technology with existing materials and by seeking new electrode materials. An alternative response to the limitations of lithium-ion batteries is to explore a new battery system with new chemistry especially electrochemistry.[9]

With the rapid advancement in the field of electronic industry and the invention of wide varieties of electronic goods, the need for a high energy to weight ratio and high electrochemical potential material was increasingly felt. The Lithium-ion batteries offer 2-3 times higher energy density and 5-6 times higher power density than conventional nickel-cadmium batteries (Ni-Cd) and nickel-metal-hydride batteries (Ni-MH). This led to the invention of Lithium-ion battery.[10] In February 1990, Sony Corporation launched first Lithium-ion Battery in the Market.[10] Since then researchers are continuously trying to develop improved version of Lithium-ion battery. Because of the reduced size of Lithium-ion batteries, it is used in mobile phones, laptops, IPods, IPads, Tablet, PCs and many more things.

The theoretical and practical energy density of different batteries and gasoline shown in Figure 1 The theoretical energy density of gasoline is 13000 $Whkg^{-1}$ and the usable (practical) energy density is approximately 1,700 $Whkg^{-1}$ according to the average tank-to-wheel efficiency of the U.S. fleet (12.1%). The energy density of current commercial lithium-ion batteries is between 100 $Whkg^{-1}$ and 200 $Whkg^{-1}$. A 10-fold improvement in energy density would be required for these batteries to replace the gasoline as a power sources for vehicles. Notably the theoretical energy density of lithium air batteries is 11680 $Whkg^{-1}$ based on the weight of lithium metal only. A practical energy density of 1,700 $Whkg^{-1}$ may be achievable for lithium-air batteries after long-term intensive work which corresponding to only 14.5 % of the theoretical energy density.[11] For the future EVs/HEVs applications a possible solution for using rechargeable Lithium-ion batteries as the power source is

to design a hybrid energy storage system that combines lithium-ion batteries (for high power density) and lithium air batteries (for high energy density).

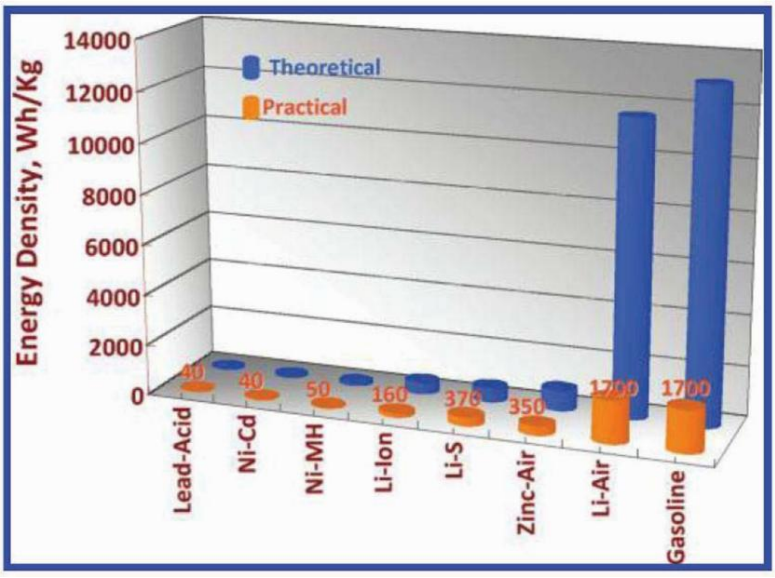

Figure 1: The gravimetric energy density ($Whkg^{-1}$) for different types of rechargeable batteries and gasoline.[11]

2.1: Lithium-ion Batteries

2.1.1: History of Lithium-ion Batteries

The Lithium-ion Battery got its name from metal of the anode (Negative electrode), Lithium, which is the most lightweight metal, the third element of the periodic table system just behind hydrogen and Helium. In the present section, history of Lithium-ion Battery has been discussed thoroughly. The major use of Lithium-ion battery is in defense sector. All superpower countries are trying to indigenously develop Lithium-ion Battery manufacturing units in their own countries. A battery is a transducer which converts chemical energy into electrical energy and vice versa. The first battery was invented in the year 1798 by Italian physicist Alessandro Volta. After a period of four decades Daniel Cell was invented. It offered better cell voltage and also eliminated the hydrogen bubble problem in Voltaic Cell. With the passage of time many important achievements took place in the history of battery development. The first was the invention of rechargeable Lead Acid cell. Until recent past an improved version of Lead Acid Cell was used as car battery. Gradually wet electrolyte cells were replaced by dry electrolyte cells. This led to the development of portable batteries. Soon after this alkaline batteries came into existence.[12,13] The lithium-ion battery has dominated the power supply market for portable devices in the past two decades since its commercialization by SONY in

February 1990. Lithium-ion Batteries have energy density 2-3 times more than conventional rechargeable batteries such as nickel-metal-hydride batteries (Ni-MH) and nickel-cadmium batteries (Ni-Cd). Lithium-ion batteries are also considered the first choice for future EVs and HEVs.

The invention of lithium-ion batteries is not an accident and it took more than two decades to bring lithium-ion batteries from the laboratory to industry. Around 1970 Gamble et al. discovered that a range of electron donating molecules and ions could be intercalated into the layered dichalcogenides.[14] Among all dichalcogenides, titanium disulfide (TiS_2) was considered to be the most promising electrode material for energy storage.[15-17] It is a semimetal with high electronic conductivity and it can form a single phase with Lithium-ions over the entire composition range of Li_xTiS_2 ($\leq[\leq 1$), enabling all the lithium to be removed reversibly.[18,19] However the low potential and high cost for production limit its commercialization.[20] Later researchers started to investigate the lithium intercalation behaviour of layered metal oxides in particular vanadium pentaoxide (V_2O_5). However, the fairly complex phase transition of V_2O_5 during lithium intercalation and poor cycling performance makes this material unsuitable for commercialization of lithium-ion batteries.[21-23] In the 1980s, Goodenough recognized that $LiCoO_2$ had a similar layered structure to the dichalcogenides and the extracted lithium could be intercalated reversibly making it a very promising electrode material.[24,25] At the same time Yazami et al. reported the reversible graphite-lithium negative electrode in a solid organic electrolyte.[26] For the carbon anode the lithium intercalation product is LiC_6. This can reduce the lithium dendritic avoiding the short circuit and makes a much safer battery than pure lithium metal. The lithium-ion battery system combining $LiCoO_2$ as the cathode materials and graphite as the anode materials was finally commercialized by SONY after more than 20 years of development.[27]

2.1.2: Basic Concepts and Principles for Lithium-ion Batteries

A rechargeable lithium-ion battery is a lithium-ion device and does not contain lithium metal. It consists of a cathode (positive electrode) and an anode (negative electrode) separated by a porous membrane soaked in a liquid organic electrolyte. Figure 2 shows a typical commercial lithium-ion battery configuration. The positive electrode (cathode) is a layered structure lithium metal oxide (e. g. $LiCoO_2$) and the negative electrode (anode) is graphite (e.g. MCMB). The electrodes are separated by a porous polymer membrane. The Li^+ conducting electrolyte is a solution of a lithium salt (e.g. $LiPF_6$) in mixed organic solvents (e.g. EC/DMC). For the charging process, Lithium-ions extract from the cathode pass through the electrolyte and intercalate into the anode. The electrons

pass through the external circuit from the negative electrode to the positive electrode. The discharge process reverses this process.

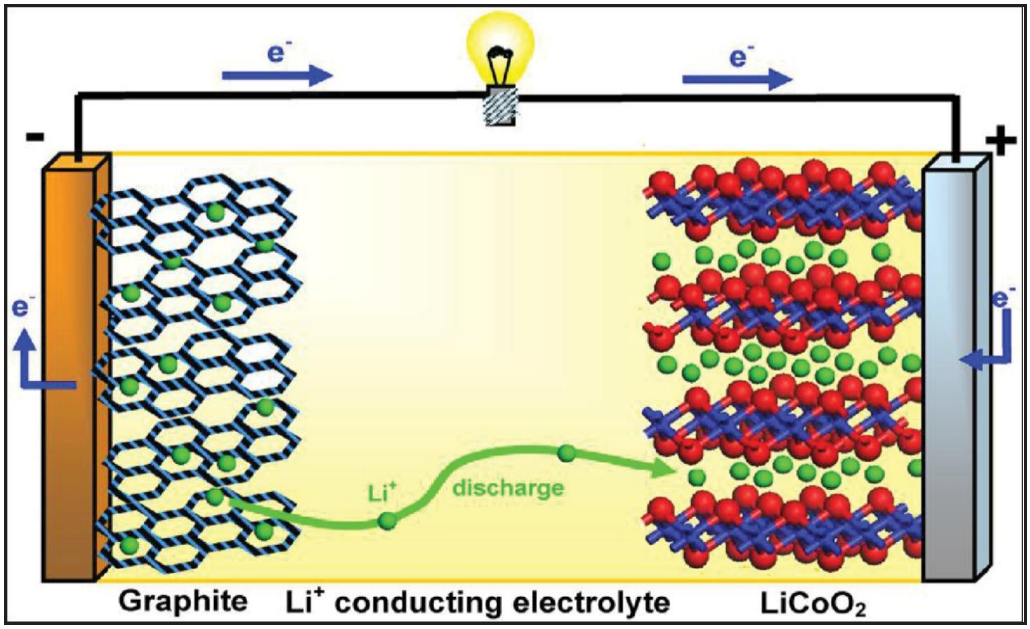

Figure 2: Schematic representation of a lithium-ion battery.[28]

The redox reaction is presented below:

$LiCoO_2 \leftrightarrow Li_{1-x}CoO_2 + xLi^+ + xe^-$ $(1<x<0)$ cathode …1

$6C + xLi^+ + xe^- \leftrightarrow Li_xC_6$ $(1<x<0)$ anode …2

The development of Lithium-ion battery broadly depends on three factors:

[1] Cathode, Anode and Electrolyte Materials.

[2] Geometry of the battery.

[3] Battery Management System.

Out of the three factors, the most important is cathode material as the discharge potential, specific capacity, cycle life etc. depends on the cathode materials.[29] The limitations of the Lithium-ion Battery are its cost and safety.[30] Table 1 summarizes the components, materials and functions of Lithium-Ion Battery. The present focus of researchers is to develop high energy density, high cycle life, economical, environment friendly and safe cathode material by various means. The present focus of researchers is to develop high energy density, high cycle life, economical, environment

friendly and safe cathode material by various means. $LiCoO_2$ was the first cathode material which was used in lithium ion battery. It is no doubt a good cathode material but has the disadvantage of being costly and toxic due to the presence of cobalt in it.

Components	Functions	Materials
Cathode	• Emit lithium-ion to anode during charging • Receive lithium-ion during discharging	lithium metal oxide powder
Anode	• Receive lithium-ion from anode during charging • Emit lithium-ion during discharging	Graphite powder
Electrolyte	• Pass lithium-ions between cathode and anode	Lithium salts and organic solvents
Separator	• Prevent short circuit between cathode and anode • Pass lithium ions through pores in separator	Micro-porous membranes

Table 1: LIB components and Functions.[30]

Some basic concepts to evaluate the electrochemical performance of lithium-ion batteries are illustrated as follows:

Cell potential: It is the potential difference between the cathode and anode materials.

Specific capacity: Specific Capacity defined the amount of electric charge the battery can store per unit mass.

The theoretical specific capacity ($Q_{TSC,}$ $mAhg^{-1}$) can be calculated from the following equation:

$$Q_{TSC} = n \times F/M \quad \ldots 3$$

Where n is the mol number of electron transfer in the electrochemical reaction, F is the Faraday constant (96,485.33 C mol^{-1}), and M is the molecular weight of the active materials.

The specific charge capacity (Q_c, $mAhg^{-1}$) or specific discharge capacity (Q_d, $mAhg^{-1}$) can be calculated from the following equation:

$$Q_c \text{ (or } Q_d) = I \times t/m \quad \ldots 4$$

Where I is the charge or discharge current (mA), t is the charge or discharge time (s), m is the mass of the active materials (g).

Specific energy: It is defined as the energy per unit mass.

Energy density: Energy density used for the amount of energy stored in a given system. The specific energy (SE, $Whkg^{-1}$) and energy density (ED, WhL^{-1}) can be calculated from the following equations:

$$SE = (E \times Q) / 1000 \quad \ldots 5$$

$$ED = (E \times Q \times m) / (100 \times V) \quad \ldots 6$$

Specific power: Specific Power is the ability of the battery to deliver power per unit mass.

Power density: Power density used for the ability of the battery to deliver power per unit volume. The specific power (SP, $Whkg^{-1}$) and power density (PD, WhL^{-1}) can be calculated from the following equations:

$$SP = SE/t \quad \ldots 7$$

$$PD = ED/t \quad \ldots 8$$

Where t is the discharge time

Irreversible capacity (Q_I): used to define the capacity loss after each cycle.

For cathode materials: $Q_I = {}^{th}Q_d - {}^{th}Q_c$ … 9

For anode materials: $Q_I = {}^{th}Q_c - {}^{th}Q_d$ …10

Coulombic efficiency: a term to represent the ratio of discharge capacity to the charge capacity.

$$\mu = {}^{th}Q_d \ / \ {}^{th}Q_c 100\% \quad \ldots 11$$

2.1.3: Selection Criteria for Lithium-ion Battery Systems

A commercial Lithium-ion battery system requires the following: [7,31]

High Cell Voltage: Most Lithium system shows a cell voltage in the upper range of 1.5 to 4.0 V or even higher. This is an advantage with regard to the energy density and specific energy of those cells. So in many cases only one Lithium cell suffices where otherwise two or three conventional Leclanche or alkaline cells are necessary.

Energy Content by Weight: Specific Energy: The mass related (gravimetric) Energy content, the 'specific Energy' (SE) of Lithium-Ion Batteries, is 100 to 500 $Whkg^{-1}$ depending on system and cell type. Preferably portable devices profit from a Lithium power supply. For comparison: classic Lead-acid Batteries show a specific energy between 35 and 55 $Whkg^{-1}$ and Nickel Cadmium Batteries, a bit more powerful, from 50 to 70 $Whkg^{-1}$. The said higher (Lithium) values have, however been only realized by primary systems until now.

Energy Content by Volume: Energy Density: The volumetric content, mostly understood as the 'Energy Density' (ED), goes from 300 to 1300 WhL^{-1}. Lithium-Ion Batteries therefore require less space than conventional Battery systems. Leclanche cells, for example deliver 165 and alkaline cell 330WhL^{-1}.

Load-ability: One can choose between Lithium primary Batteries tailor-made as high rate batteries with a very low resistance for high loads or with a high resistance for low rate long time application.

Charge and Discharge Characteristic: Some Lithium systems show an especially flat and stable curve (between Voltage and time) for the discharge of the whole Capacity. Its support electronic device which is designed for little tolerances of their feeding voltages. A general lithium-Ion battery must be capable of complete charge and discharge over 300 cycles with capacity loss less than 20%. For automotive applications, the cycle life should be more than 2000 cycles.

Deep Temperature Capability: For a general consumer battery, the battery operation temperature should be in the range of -10^0C to -40^0C and the storage temperature should be in the range of -20 to 85^0C.

Shelf Life: Most of the Lithium-ion Batteries may be stored for over 10 up to 20 years with negligible self-discharge, So that they still deliver most of their normal capacity. All commercial batteries must be safe in the normal operating environment. They are continuously active, i.e. at all time ready for service. At normal temperature storage only 5 to 10% self-discharge after 10 years is typical, and cost of the battery should be affordable for the customer.

Stability and Environmental Compatibility: The materials must maintain their mechanical and chemical stability over time in the operating environment, avoiding, for example, reaction with the electrolyte or no irreversible phase change. If compared to metals used for common batteries such as Lead or nickel and Cadmium, Lithium should not vent hazardous materials, nor present any hazard

under mild abuse conditions (e.g. leaking, explosion, etc). Disposal of used Lithium-ion Batteries is therefore a smaller problem.

2.2: Nanostructure Electrode Materials for Lithium-ion Batteries

Although the present commercial lithium-ion batteries are successful especially in small portable devices, they still need to conquer very big challenges for high power applications such as EVs and HEVs. The commercial lithium-ion batteries are based mainly on micro-sized electrode materials. In the solid state intrinsic lithium-ion diffusion coefficient is less than 10^{-8} cm^2S^{-1}, which significantly limits the rate of lithium ion intercalation/de-intercalation from the solid state, and hence the charge/discharge rate performance. Nanostructure materials instead of the current micro-sized electrode materials is considered to be the most promising strategy for overcoming the current limits: the reduced dimensions can greatly shorten the lithium ion diffusion path and enable far higher intercalation/deintercalation rates and hence high power.[2] The advantages of nanostructure electrode materials for rechargeable lithium-ion batteries are given below.[32,33]

Advantages

1. Due to the Reduction in the particle size to nanoscale significantly reduces the lithium-ion diffusion distance within the particles. The characteristic time constant for diffusion is calculated by $\tau = L^2/D$, where L is the diffusion length and D is the diffusion constant. The time for lithium-ion intercalation/de-intercalation decreases with the square of the particle size that shows the remarkable effect of replacing micro-sized with nanostructure sized particles.

2. electron transport within the particles is also increased by nano dimension particles that is described for lithium-ions transportation.[2]

3. Nanostructure material with a high surface area allows a very high contact area between electrode and electrolyte and hence the number of active sites for electrode reactions, which in turn decreases electrode polarization loss and improves the power density.

4. Nanostructure materials with new lithium storage mechanisms can achieve much higher capacities than conventional micro structural intercalation materials. present studies show that excess lithium ions can be stored on the surface, interface,[34-36] and in nanopores.[37-39]

5. It has been found that nanosized electrode materials become active for lithium-ion insertion, that is unable to take place in bulk form.[2,40]

6. The redox potentials for lithium Ions and electrons can be modified by nanostructures, resulting in a change of cell voltage.[41,42]

7. Nanostructure materials could more easily accommodate the strain associated with lithium intercalation/de-intercalation.[43,44]

2.3: Nanostructure Cathode Materials

In a lithium-ion battery, the cathode material is the active materials in the positive electrode. it is associated with the oxidation reaction and during the cell discharge process it gains electrons from the external circuit. a good cathode material for a lithium-ion battery should have the following requirements:

1. The material should react with lithium-ion reversibly and contain a readily ion, and readily ion can participate in the redox reaction.

2. The material should have a very high free energy to react with lithium to supply a high discharge voltage.

3. The material should have very high electronic conductivity for electron transportation and very high ionic conductivity for lithium-ion transportation.

4. The material should be stable and safe during the entire operation environment.

5. The material should be low cost and friendly to the environment.

2.4: Nanostructure Layered Oxides

The first Nanostructure Layered oxide Material report by Goodenough in 1980.[24] The layered metal oxides such as $LiCoO_2$, $LiNiO_2$, $LiMnO_2$, $LiNi_{1/2}Mn_{1/2}O_2$ and $LiNi_{1/3}Mn_{1/3}Co_{1/3}O_2$, have received tremendous attention as cathode materials for lithium-Ion batteries. In February 1990, SONY Corporation launched first lithium-ion battery in market. The safety aspect of the battery during its operation was major issue, because of the presence of Lithium in its metallic form as one electrode. However, such problem was sorted out with the invention of graphite material which acts as lithium

host. After successfully intercalations and deintercalations of lithium into graphite which has layered structure, LiC_6 was used as anode. This is much safer anode material because lithium, unlike metallic form, is present in the form of Ion in the compound. On the other hand, $LiCoO_2$ has been used as the conventional cathode materials because of its Layered Structure. $LiCoO_2$ cathode with a graphite anode to make the first commercial lithium-Ion batteries and this configuration still dominates the lithium battery market. The $LiCoO_2$ cathode had an α-$NaFeO_2$-type structure with the oxygen in a cubic close-packed arrangement and it showed that lithium can be extracted reversibly (Figure 3).[45, 46]

Although the theoretical specific capacity of $LiCoO_2$ is 274 $mAhg^{-1}$ it can only achieve a practical capacity of about 140 $mAhg^{-1}$. The electrochemical and in situ X-ray diffraction studies showed that Lithium-ion ordering occurs at x=0.5, which coupled to a lattice distortion from hexagonal to monoclinic symmetry.[45] The complete removal of lithium from $LiCoO_2$ will cause the oxygen layers to rearrange giving hexagonal close packing oxygen to CoO_2.[22] The Lithium-ion diffusion coefficient of $LiCoO_2$ is 5×10^{-9} cm^2s^{-1} which is comparable with $LiTiS_2$ (10^{-8} cm^2s^{-1}).[20] However, the conductivity of Li_xCoO_2 can dramatically change by 2~4 orders of magnitude at ambient temperatures from metal-like material to a typical semiconductor.[47,48] To improve the electrochemical performance nanostructure $LiCoO_2$ has been synthesized and developed. The first strategy was surface modification.[49] Nano-sized carbon coating on $LiCoO_2$ from the decomposition of sucrose showed a higher capacity and lower charge transfer resistance than pristine $LiCoO_2$.[50] Coating a nanolayer metal oxide or phosphate on the surface of the $LiCoO_2$ particles can also significantly improve the capacity. Cho et al. reported that ZrO_2 coated $LiCoO_2$ can deliver a discharge capacity of 170 $mAhg^{-1}$ when cycled between 2.75 and 4.4 V at room temperature without capacity loss over 70 cycles.[51] Kim et al. reported the $LiCoO_2$ particles coated by $AlPO_4$ can significantly improve the safety for lithium-Ion batteries and also exhibited the highest intercalation capacity (230 $mAhg^{-1}$) in a voltage range of 4.8 and 3 V at a rate of 0.1 C.[52,53] A thin-film coating of metal oxide or metal phosphate on the $LiCoO_2$ particles can suppresses the cobalt dissolution and phase transitions caused by the lattice-constant changes during electrochemical cycling.

The model of the Layered $LiCoO_2$ is shown in Figure 3(a). And Layered structure with space group R3m is shown in figure 3(b).The high cost and the safety problem of $LiCoO_2$ limits its application to large-scale lithium power batteries for EVs and HEVs. The layered materials oxides such as $LiNiO_2$ and $LiMnO_2$ have been extensively studied as an alternative cathode material for $LiCoO_2$.[54-56] but they posses various practical limitations, such as the difficulty to synthesize phase pure materials,

structure changes during the cycling, thermal instability of $LiNiO_2$ and structural degradation of $LiMnO_2$.[57]

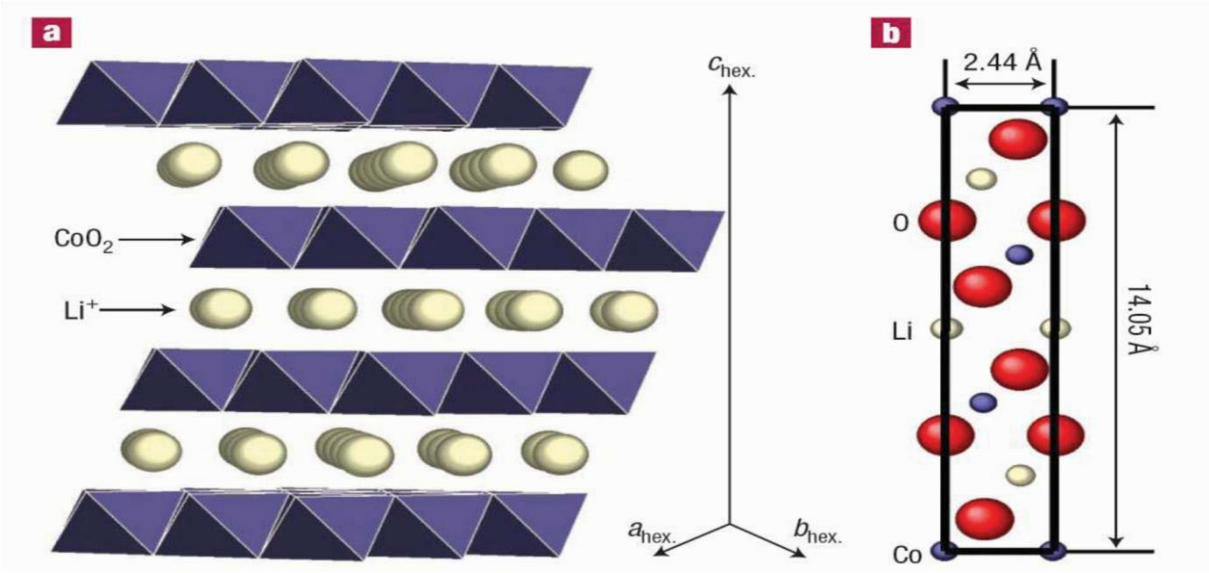

Figure 3(a): Models of the layered $LiCoO_2$ Figure 3(b): structure with space group $R\bar{3}m$.[46]

Ohzuku et al. proposed the new layered materials $LiNi_{1/2}Mn_{1/2}O_2$ and $LiNi_{1/3}Mn_{1/3}Co_{1/3}O_2$ which were synthesized by the Co-Precipitation Method. And Ohzuku et al. reported that the electrochemical performance of $LiCoO_2$ can be improved by multi-substitution to form $LiNi_{1/3}Mn_{1/3}Co_{1/3}O_2$ and that the safety can be improved by further doping with Al, making $LiNi_{1/3}Mn_{1/3}Co_{1/3}O_2$ a potential cathode material for lithium-ion power batteries.[60-62]

Kaliyappan et al. have reported that $Li_{1+x}\{Mn_{0.4}Ni_{0.4}Fe_{0.2}\}_{1-x}O_2$ (x=0.2) Li^+ exhibits a good electrochemical property with maximum initial capacity of 160 $mAhg^{-1}$ between 2- 4.5 V at 0.1 $mAcm^{-2}$ current density and the capacity retention after 25 cycles was 92%.[68] This layered materials containing iron could be used as low cost and eco-friendly energy source materials for large scale Lithium-ion batteries application.

2.5: Synthesis of $Li_{1+x}M_{1-x}O_2$ [M=Mn, Ni, Fe and x=0.2]

$Li_{1+x}M_{1-x}O_2$ [M=Mn, Ni, Fe and x=0.2] can be synthesized by different methods. Each method has some advantages and disadvantages associated with it. Depending upon the synthesis process different structure and characteristics are obtained. In this section a comparative study has been done. The main synthesis processes are:

1. Solid State Method
2. Microwave Method
3. Hydrothermal Method
4. Carbothermal Reduction
5. Sol-Gel Method

Table 2 shows the comparison of different synthesis process.

	Solid-state method	Sol–gel processing	Microwave processing	Hydrotheral reaction	Crabothermal reduction	Spray pyrolysis
Purity	Low	High	Moderate	High	High	High
Particle size	Digger	50–150 nm	40–50 nm	Bigger	100–300 nm	40–200 nm
Agglomeration	Yes	No	Yes	No	No	No
Complication degree of equipment	Simple	Simple	Simple	Complicate	Simple	Complicate
Reactive period	Long	Long	Short	Moderate	Long	Short
Energy consumption	High	Low	Low	High	High	Low
Reaction control	Easy	Easy	Difficult	Easy	Easy	Difficult
Industrialization	Easy	Difficult	Difficult	Difficult	Difficult	Difficult
Performance	Low	Good	Moderate	Moderate	Good	Moderate

Table 2: Comparison of different synthesis process.[63]

2.5.1: Sol-Gel Method

Sol-Gel is wet-chemical-based self assembly process for nano-material formation. The Sol-Gel process, as name implies, involves the evolution of networks through the formation of a colloidal suspension (sol) and gelation of the sol to form a network in a continuous liquid phase (gel). The precursors used for synthesizing the colloidal generally consist of metallic ions and ligands which are elements surrounded by various reactive species. The gelation is done by the chelating agent such as citric acid, adipic acid or ascorbic acid. The chelating agent forms an interconnected structure with pores made up of sol particles. Because of this reason it is known as sol gel method. The sol gel is heated at 80^0C to form xerogel. The xerogel is then calcined at around 750^0C to form $Li_{1+x}M_{1-x}O_2$ [M=Mn, Ni, Fe and x=0.2].

In general, sol-gel formation occurs in four steps:

1. Hydrolysis and alcoholysis.
2. Water and alcohol condensation and polymerization of monomers to form particles.

3. Growth of particles.

4. Agglomeration of particles followed by the formation of networks throughout the liquid medium resulting in thick gel.

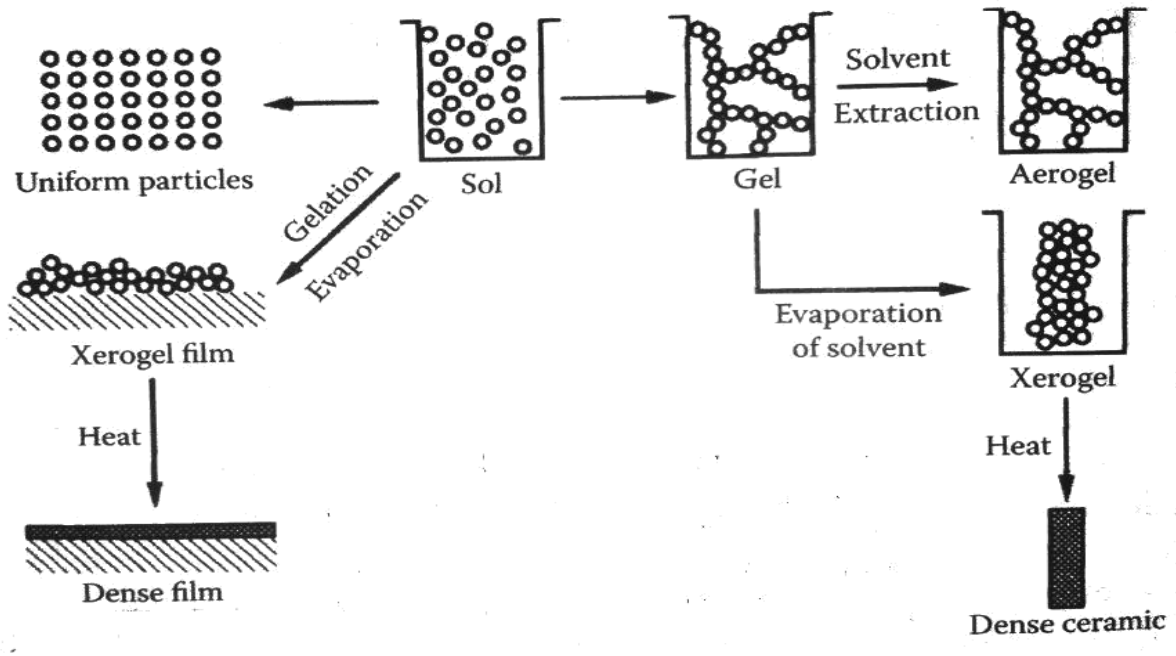

Figure 4: chemical synthesis by sol-gel route.[64]

Sol Gel Method has the following advantages:

1. Reaction parameters, such as temperature, time, pH, precursor, solvent, concentration, and viscosity, etc., are of importance for the formation and ultimate morphology (particle size and shape, pore size, and porosity) of the obtained powders.

2. Sol-Gel is a low cost method.

3. Sol Gel Method produces Micropores which increases the conductivity.

4. High purity, uniform structure and very small size is obtained.

5. Because of these advantages sol gel method has been chosen as the synthesis method.

2.6: Optimization of $Li_{1+x}M_{1-x}O_2$ [M=Mn, Ni, Fe and x=0.2]

The current situation demands the design of new cathode materials for Lithium-ion battery which would provide high cell voltage, high life cycle, high specific energy, and high power density and at

the same time it has to be economical. $LiCoO_2$ showed excellent electrochemical behaviour, the high cost and toxicity of cobalt leads to lookout for the alternatives such as $LiMnO_2$ although there has been much works focused on the optimization of manganese.[65-68] it was found that $LiMnO_2$ was suitable cathode material which can potentially replace $LiCoO_2$. $LiMnO_2$, with its higher capacity (280 mAh/g), lower price and Environmental Friendliness, seem to be an attractive alternative cathode material for Lithium-ion Batteries. This Material, however, is structurally unstable, which implies insufficient cyclability of manganese oxide based batteries. There have been numerous attempts to improve its structural stability. Addition of extra lithium will tend to push the manganese away from trivalent to tetravalent.[69] thus minimizing the impact of any Jahn-Teller distortion coming from Mn^{3+}.it was found that by manganese substitution with Nickel and Iron improved the structural stability. From our investigation of literature, it was found that nickel and Iron doped $Li_{1+x}Mn_{1-x}O_2$ (x=0.2) having general formula $Li_{1+x}\{Mn_{0.4}Ni_{0.4}Fe_{0.2}\}_{1-x}O_2$ (x=0.2) has the potential to fulfill the above criteria. Hence sol gel is opted for synthesis of these compounds. The layered Material $Li_{1+x}\{Mn_{0.4}Ni_{0.4}Fe_{0.2}\}_{1-x}O_2$ with (x=0.2) exhibited excellent electrochemical performance with maximum initial capacity and enhanced cyclic behavior. this improved performance was attributed to its well ordered layered structure and small particles with uniform size distribution.

Kaliyappan et al. have reported that $Li_{1+x}\{Mn_{0.4}Ni_{0.4}Fe_{0.2}\}_{1-x}O_2$ (x=0.2) Li^+ exhibits a good electrochemical property with maximum initial capacity of 160 $mAhg^{-1}$ between 2- 4.5 V at 0.1 $mAcm^{-2}$ current density and the capacity retention after 25 cycles was 92%.[68] This layered materials containing iron could be used as low cost and eco-friendly energy source materials for large scale Lithium-ion batteries application. Hence, sol-gel is opted for synthesis of these compounds.

CHAPTER-3: SYNTHESIS AND CHARACTERIZATION

3.1: Synthesis of $Li_{1+x}Mn_{1-x}O_2$ (x=0.2)

Synthesis of $Li_{1+x}Mn_{1-x}O_2$ (x=0.2) was carried out by stoichiometric amount of lithium acetate [$Li(CH_3COO).2H_2O$], manganese Acetate [$Mn(CH_3COO)_2.4H_2O$] compounds and these compounds were dissolved in triply distilled water unless these were completely dissolved and then added to a continuously stirred aqueous solution containing Citric acid (weighing double the mass of lithium acetate [$Li(CH_3COO).2H_2O$] and manganese Acetate $Mn(CH_3COO)_2.4H_2O$ collectively) as chelating agent. These three solutions were then mixed together and the pH of the mixed solution was maintained in between 6-7 by adding NH_4OH solution. The resulting solution was heated at 80^0C in a magnetic stirrer unless a transparent gel was obtained. After the evaporation of water, the gel turned into a viscous transparent gel. The resulting precursor was decomposed at 350^0C for 5 hours in air environment to eliminate the organic moieties, such as acetate and carboxylic groups. The decomposed powder were ground, and kept into the furnace for calcinations at 750^0C for 12 hours in air atmosphere to obtained nanocrystalline powders.

The formation of desired phase of the synthesized powder was confirmed by X-ray diffraction measurement using $CuK\alpha_1$ radiation in conjunction with nickel filter by Bruker make D8 ADVANCE model. The wide range XRD pattern was obtained between 10^0 and 70^0 at scan rate of 2^0 min^{-1} at an applied potential of 40 KV and current of 30 mA.

The Micro structural investigation such as morphology, particle size and distribution of particles in surface and subsurface region of the calcined powder was performed using Hitachi make model S-4700 of scanning electron microscope, and the elemental analysis of the calcined powder was performed using Energy-dispersive X-ray spectroscopy (EDS).

Impedance measurements were carried out by making pellets of calcined powder of diameter, 1.0 cm and thickness, 2.03 mm at room temperature using LCR METER (Agilent 4284A) in the frequency range of 20 Hz to 1 MHz, for making pellet we used polyvinyl alcohol (PVA) as binder and then heated at 400^0C to remove moisture. The flat surface of the pellet was coated with gold for making conductive surface. All the measurement has been done at biased voltage one volt. Synthesis process of $Li_{1+x}Mn_{1-x}O_2$ (x=0.2) shown in figure.

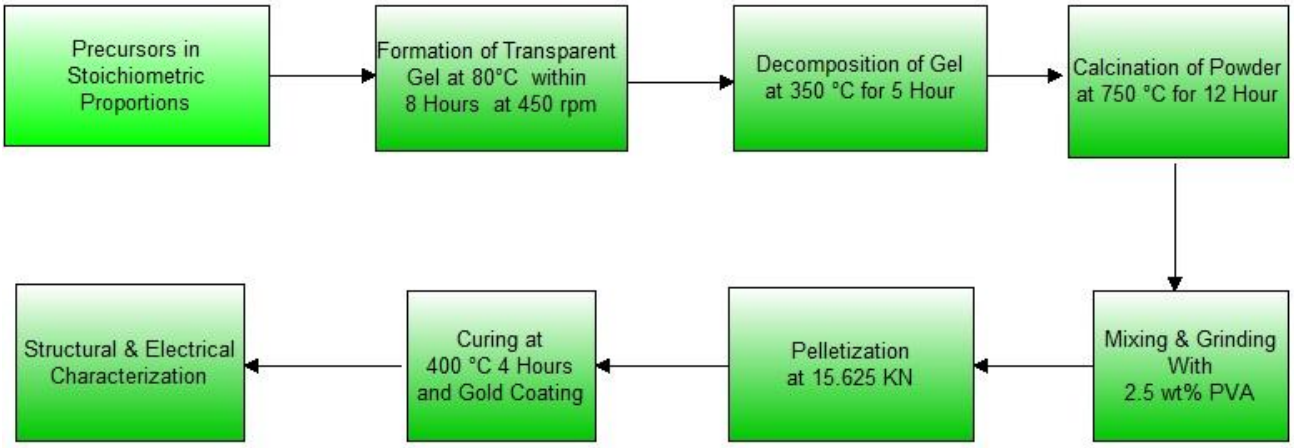

Figure 5: Synthesis process of $Li_{1+x}Mn_{1-x}O_2$ (x=0.2) calcined at 750^0C for 12 hours in air

3.2: Synthesis of $Li_{1+x}\{Mn_{0.4}Ni_{0.4}Fe_{0.2}\}_{1-x}O_2$ (x=0.2) in air atmosphere

Synthesis of $Li_{1+x}\{Mn_{0.4}Ni_{0.4}Fe_{0.2}\}_{1-x}O_2$ (x=0.2) was carried out by stoichiometric amount of lithium acetate [$Li(CH_3COO).2H_2O$], manganese Acetate [$Mn(CH_3COO)_2.4H_2O$] Nickel Acetate [$Ni(CH_3COO)_2.H_2O$] and Ferric nitrate [$Fe(NO_3)_3.9H_2O$] compounds and these compounds were dissolved in triply distilled water unless these were completely dissolved and then added to a continuously stirred aqueous solution containing Citric acid (weighing double the mass of lithium acetate [$Li(CH_3COO).2H_2O$], manganese Acetate [$Mn(CH_3COO)_2.4H_2O$] and Ferric nitrate [$Fe(NO_3)_3.9H_2O$] collectively) as chelating agent. These three solutions were then mixed together and the pH of the mixed solution was maintained in between 6-7 by adding NH_4OH solution. The resulting solution was heated at 80^0C in a magnetic stirrer unless a transparent greenish gel was formed. After the evaporation of water, the gel turned into a viscous transparent gel. The resulting precursor was decomposed at 350^0C for 5 hours in air environment in eliminate the organic moieties, such as acetate carboxylic groups. The decomposed powder were ground, and kept into the furnace for calcinations at 750^0C for 14 hours in air atmosphere to obtained nanocrystalline powders.

The formation of desired phase of the synthesized powder was confirmed by X-ray diffraction measurement using $CuK\alpha_1$ radiation in conjunction with nickel filter by Bruker make D8 ADVANCE model. The wide range XRD pattern was obtained between 10^0 and 70^0 at scan rate of 2^0 min^{-1} at an applied potential of 40 KV and current of 30 mA.

The Micro structural investigation such as morphology particle size and distribution of particles in surface and subsurface region of the calcined powder was performed using Hitachi make model S-

4700 of scanning electron microscope, and the elemental analysis of the calcined powder was performed using Energy-dispersive X-ray spectroscopy (EDS).

Impedance measurements were carried out by making pellets of calcined powder of diameter, 1.0 cm and thickness, 1.98 mm at room temperature using LCR METER (Agilent 4284A) in the frequency range of 20 Hz to 1 MHz, for making pellet we used polyvinyl alcohol (PVA) as binder and then heated at 400^0C to remove moisture. The flat surface of the pellet was coated with gold for making conductive surface. All the measurement has been done at biased voltage one volt. Synthesis process of $Li_{1+x}\{Mn_{0.4}Ni_{0.4}Fe_{0.2}\}_{1-x}O_2$ (x=0.2) shown in figure.

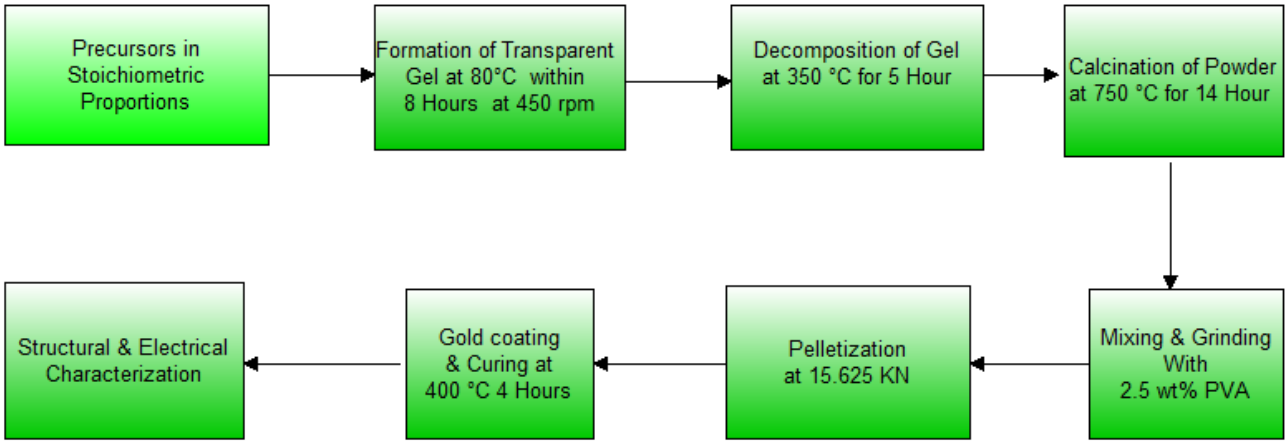

Figure 6: Synthesis Process of $Li_{1+x}\{Mn_{0.4}Ni_{0.4}Fe_{0.2}\}_{1-x}O_2$ (x=0.2) calcined at 750^0C for 14 hours in air

3.3: Synthesis of $Li_{1+x}\{Mn_{0.4}Ni_{0.4}Fe_{0.2}\}_{1-x}O_2$ (x=0.2) in inert atmosphere

Synthesis of $Li_{1+x}\{Mn_{0.4}Ni_{0.4}Fe_{0.2}\}_{1-x}O_2$ (x= 0.2) was carried out by stoichiometric amount of lithium acetate [$Li(CH_3COO).2H_2O$], manganese Acetate [$Mn(CH_3COO)_2.4H_2O$] Nickel Acetate [$Ni(CH_3COO)_2.H_2O$] and Ferric nitrate [$Fe(NO_3)_3.9H_2O$] compounds and these compounds were dissolved in triply distilled water unless these were completely dissolved and then added to a continuously stirred aqueous solution containing Citric acid (weighing double the mass of lithium acetate [$Li(CH_3COO).2H_2O$], manganese Acetate [$Mn(CH_3COO)_2.4H_2O$] and Ferric nitrate [$Fe(NO_3)_3.9H_2O$] collectively) as chelating agent. These three solutions were then mixed together and the pH of the mixed solution was maintained in between 6-7 by adding NH_4OH solution. The resulting solution was heated at 80^0C in a magnetic stirrer unless a transparent greenish gel was formed. After the evaporation of water, the gel turned into a viscous transparent gel. The resulting precursor was decomposed at 350^0C for 5 hours in inert environment in eliminate the organic

moieties, such as acetate carboxylic groups. The decomposed powder were ground, and kept into the furnace for calcinations at 750^0C for 12 hours in inert atmosphere to obtained nanocrystalline powders.

The formation of desired phase of the synthesized powder was confirmed by X-ray diffraction measurement using $CuK\alpha_1$ radiation in conjunction with nickel filter by Bruker make D8 ADVANCE model. The wide range XRD pattern was obtained between 10^0 and 80^0 at scan rate of 2^0 min^{-1} at an applied potential of 40 KV and current of 30 mA.

The Micro structural investigation such as morphology, particle size and distribution of particles in surface and subsurface region of the calcined powder was performed using Hitachi make model S-4700 of scanning electron microscope, and the elemental analysis of the calcined powder was performed using Energy-dispersive X-ray spectroscopy (EDS).

Impedance measurements were carried out by making pellets of calcined powder of diameter, 1.0 cm and thickness, 1.88 mm at room temperature using LCR METER (Agilent 4284A) in the frequency range of 20 Hz to 1 MHz for making pellet we used polyvinyl alcohol (PVA) as binder and then heated at 400^0C to remove moisture. The flat surface of the pellet was coated with gold for making conductive surface. All the measurement has been done at biased voltage one volt. Synthesis process of $Li_{1+x}\{Mn_{0.4}Ni_{0.4}Fe_{0.2}\}_{1-x}O_2$ (x=0.2) shown in figure.

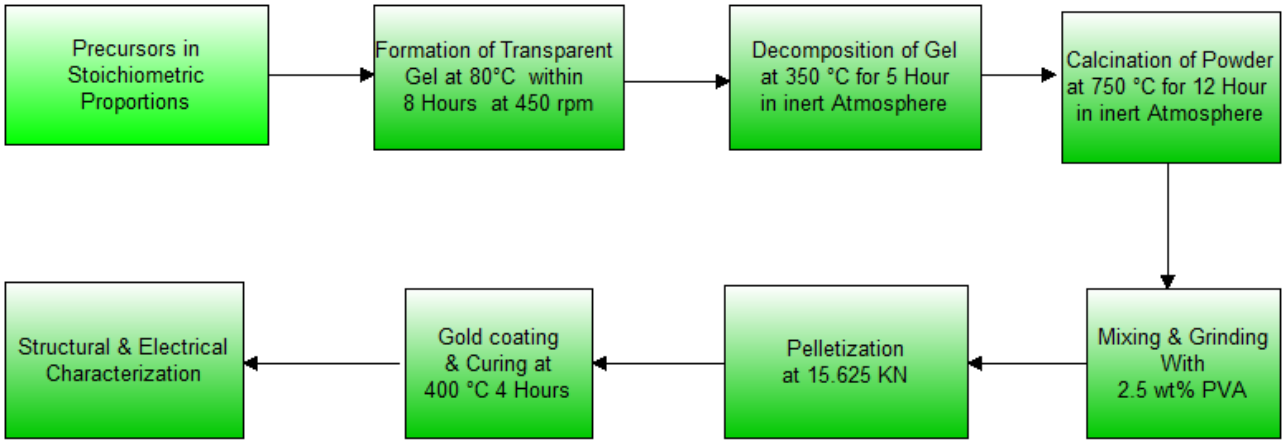

Figure 7: Synthesis Process of $Li_{1+x}\{Mn_{0.4}Ni_{0.4}Fe_{0.2}\}_{1-x}O_2$ (x=0.2) calcined at 750^0C for 12 hours in inert atmosphere

3.4: Experimental Setup

3.4.1: Magnetic Stirrer with Hot Plate

Figure 8: Magnetic stirrer with Hot Plate

The 'MLH' series magnetic stirrers with hot plate have additional stainless steel hot plate. PMDC motor gives higher torque even at lower speeds and maintains speed stability despite viscosity or volume changes. Accurate steeples speed control allows smooth variation up to 1200 rpm. Heating energy is controlled by energy regulator. The 'MLH' series magnetic stirrers content Salient Features:

1. PMDC motor for higher torque even at low speeds.
2. Better low speed stirring even with small volume.
3. Accurate steeples speed control maintains excellent speed stability.

Synthesis of $Li_{1+x}Mn_{1-x}O_2$ (x=0.2) was carried out by stoichiometric amount of lithium acetate [$Li(CH_3COO).2H_2O$], manganese Acetate [$Mn(CH_3COO)_2.4H_2O$] compounds and these compounds were dissolved in triply distilled water unless these were completely dissolved and then added to a continuously stirred aqueous solution containing Citric acid (weighing double the mass of lithium acetate [$Li(CH_3COO).2H_2O$] and manganese Acetate $Mn(CH_3COO)_2.4H_2O$ collectively) as chelating agent. These three solutions were then mixed together and the pH of the mixed solution was maintained in between 6-7 by adding NH_4OH solution. The resulting solution was heated at 80^0C-90^0 C in a magnetic stirrer unless a transparent gel was obtained.

Synthesis of Synthesis of $Li_{1+x}\{Mn_{0.4}Ni_{0.4}Fe_{0.2}\}_{1-x}O_2$ (x=0.2) was carried out by stoichiometric amount of lithium acetate [$Li(CH_3COO).2H_2O$], manganese Acetate $Mn(CH_3COO)_2.4H_2O$ Nickel

Acetate [$Ni(CH_3COO)_2.H_2O$] and Ferric nitrate [$Fe(NO_3)_3.9H_2O$] compounds and these compounds were dissolved in triply distilled water unless these were completely dissolved and then added to a continuously stirred aqueous solution containing Citric acid (weighing double the mass of lithium acetate [$Li(CH_3COO).2H_2O$], manganese Acetate [$Mn(CH_3COO)_2.4H_2O$] and Ferric nitrate [$Fe(NO_3)_3.9H_2O$] collectively) as chelating agent. These three solutions were then mixed together and the pH of the mixed solution was maintained in between 6-7 by adding NH_4OH solution. The resulting solution was heated at 80^0C-90^0 C in a magnetic stirrer unless a transparent greenish gel was formed.

3.4.2: Mortar and Pestle

Figure 9: Mortar and Pestle

The mortar is a bowl, typically made of hard wood, ceramic or stone. The pestle is a heavy club-shaped object. An agate mortar and pestle was used to grind xerogel into fine powder. Agate is a microcrystalline variety of SiO_2.

3.4.3: Alumina Tube

Alumina (Al_2O_3) has a high melting point around 2072^0C. It is used in furnace as a tube material.

3.4.4: Automatic Temperature Controlled Tubular Furnace

Figure 10: Automatic Temperature Controlled Tubular Furnace

The above experimental set up was used to perform decomposition and calcinations. This set up consisted of an alumina tube, a furnace, a digital temperature controller, variac, relay, and ammeter, Nitrogen and argon cylinder as well.

3.4.5: Furnace

The furnace could go up to a maximum of 1250^0C.

3.4.6: Digital Temperature Controller

The required temperature in a digital temperature controller was adjusted manually. The controller had a thermocouple based sensor feedback system which sends a current signal proportional to the difference in temperature inside the furnace and outside the furnace. When the temperature difference becomes zero, it sends a signal to the relay and it switched off.

3.4.7: Relay

The relay was connected in between the variac and the furnace. It was also connected to the digital temperature controller. DTC sent signal to relay when specified temperature was obtained. In this way the relay was working as a switch.

3.4.8: Variac

The variac gave output voltage in between 0 to 300 Volts for 240 Volt input supply.

3.5: Characterization Techniques

In order to investigate various properties of the prepared sample, it has to goes under a number of characterisation techniques. The result gives the information about the different optical, electrical as structural properties of sample.

3.5.1: Structural and Morphological Characterization

Structural characterisation is done to get exact information about the crystal structure, surface morphology, particle size etc the following techniques are available.

1. XRD (X-ray Diffraction)
2. SEM (Scanning electron microscope)

3.5.2: Electrical Characterization

1. Impedance Analyzers (LCR meter)

3.5.1.1: XRD (X-ray Diffraction)

Up to 1895 the study of matter at the atomic level was a difficult task but the discovery of electromagnetic radiation with 1 Å (10^{-10} m) wavelength, appearing at the region between gamma-rays and ultraviolet, makes it possible. As the interatomic distance in matter is comparable with the wavelength of X-ray, the phenomenon of diffraction find its way through it and gives many promisable results related to the crystalline structure.

Crystals are regular arrays of atoms, and X-rays can be considered waves of electromagnetic radiation. Atoms scatter X-ray waves, primarily through the atoms' electrons. Just as an ocean wave striking a lighthouse produces secondary circular waves emanating from the lighthouse, so pan X-ray striking an electron produces secondary spherical waves emanating from the electron. This phenomenon is known as elastic scattering, and the electron (or lighthouse) is known as the scatterer. A regular array of scatterers produces a regular array of spherical waves. Although these waves cancel one another out in most directions through destructive interference, they add constructively in a few specific directions, determined by Bragg's law.

$$2d \sin\theta = n\lambda \qquad \ldots 12$$

Where n is an integer 1, 2, 3…….λ is wavelength in angstroms (1.542 Å for copper), d is interatomic spacing in A°, and θ is the diffraction angle in degrees. The characteristic of the sample can be determined by plotting the angular positions and intensities of the resultant diffracted peaks of radiation. XRD is used to determine the structure of sample, i.e. how the atoms pack together in the crystalline state and what the interatomic distances and angle are.

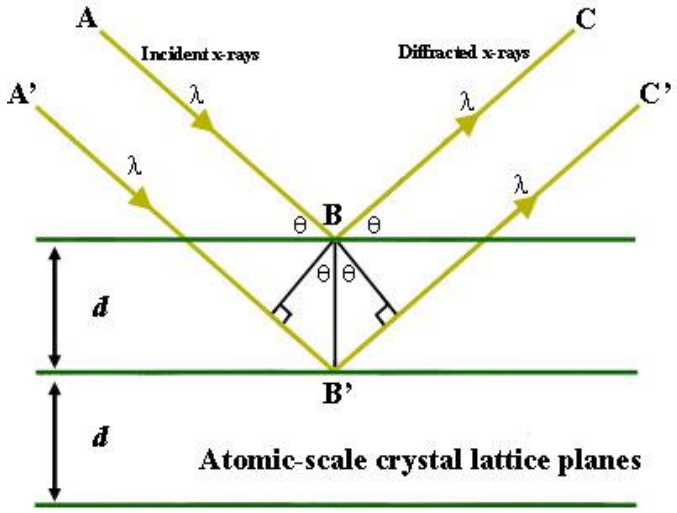

Figure 11: X-Ray diffraction in accordance with Bragg's law.[70]

The main components of XRD are an X-ray tube, a sample holder, and an X-ray detector. X-rays are generated by in a cathode ray tube by heating a filament to produce electrons, accelerating the electrons toward a target by applying a voltage, and bombarding the target material with electrons. When electrons have sufficient energy to dislodge inner shell electrons of the target material, characteristic X-ray spectra are produced. These spectra consist of several components, the most common being K_{α} and K_{β}. K_{α} consists, in part, of $K_{\alpha 1}$ and $K_{\alpha 2}$. $K_{\alpha 1}$ has a slightly shorter wavelength and twice the intensity as $K_{\alpha 2}$. The specific wavelengths are characteristic of the target material (Cu, Fe, Mo, Cr). Filtering, by foils or crystal monochrometers is required to produce monochromatic X-rays needed for diffraction. $K_{\alpha 1}$and $K_{\alpha 2}$ is sufficiently close in wavelength such that a weighted average of the two is used. Copper is the most common target material for single-crystal diffraction, with Cu K_{α} radiation = 1.5418Å.[70] These X-rays are collimated and directed onto the sample. As the sample and detector are rotated, the intensity of the reflected X-rays is recorded. When the geometry of the incident X-rays impinging the sample satisfies the Bragg Equation, constructive interference occurs and a peak in intensity occurs. A detector records and processes this X-ray signal and converts the signal to a count rate which is then output to a device such as a printer

or computer monitor. The geometry of an X-ray diffractometer is such that the sample rotates in the path of the collimated X-ray beam at an angle θ while the X-ray detector is mounted on an arm to collect the diffracted X-rays and rotates at an angle of 2θ. The instrument used to maintain the angle and rotate the sample is termed a goniometer. For typical powder patterns, data is collected at 2θ from ~5° to 80°, angles that are preset in the X-ray scan. The figure below shows the X-Ray diffractometer Brucker D8 advance available in Delhi Technological University.

Figure 12: XRD (X-ray Diffraction) Bruker D8 Advance

3.5.1.2: SEM (Scanning electron microscope)

A scanning electron microscope (SEM) is a type of electron microscope that uses backscattered electron from a sample for imaging. Scanning Electron can be used to image of the thick surface. The electrons interact with atoms in the sample, producing various signals that can be detected and that contain information about the sample's surface topography and composition. The signals that derive from electron reveal information about the sample including external morphology (texture), chemical composition, and crystalline structure and orientation of materials making up the sample. In most applications, data are collected over a selected area of the surface of the sample, and a 2-dimensional image is generated that displays spatial variations in these properties. The electron beam is generally scanned in a raster scan pattern, and the beam's position is combined with the detected signal to produce an image. The SEM is an instrument that produces a largely magnified image by using electrons instead of light to form an image. A beam of electrons is produced at the top of the microscope by an electron gun. The electron beam follows a vertical path through the

microscope, which is held within a vacuum. The beam travels through electromagnetic fields and lenses, which focus the beam down toward the sample. Once the beam hits the sample, electrons and X-rays are ejected from the sample. Specimen interaction is what makes electron microscopy possible. The energetic electron in the microscope strike the sample and various reactions can occurs as shown in figure. The reaction noted on the top side of the diagram are utilized when examining thick or bulk specimen (SEM) while the reactions on the bottom side are those examined in thin or foil specimen (TEM). A diagram showing the generation depths of the interactions is also given in diagram. Probe current means an electron beam focused on the specimen. Working with specimen, probe current emits electron containing information on the specimen such as secondary electron and backscattered electron. The size of probe current determined the number of secondary electron and backscattered electron emitted.

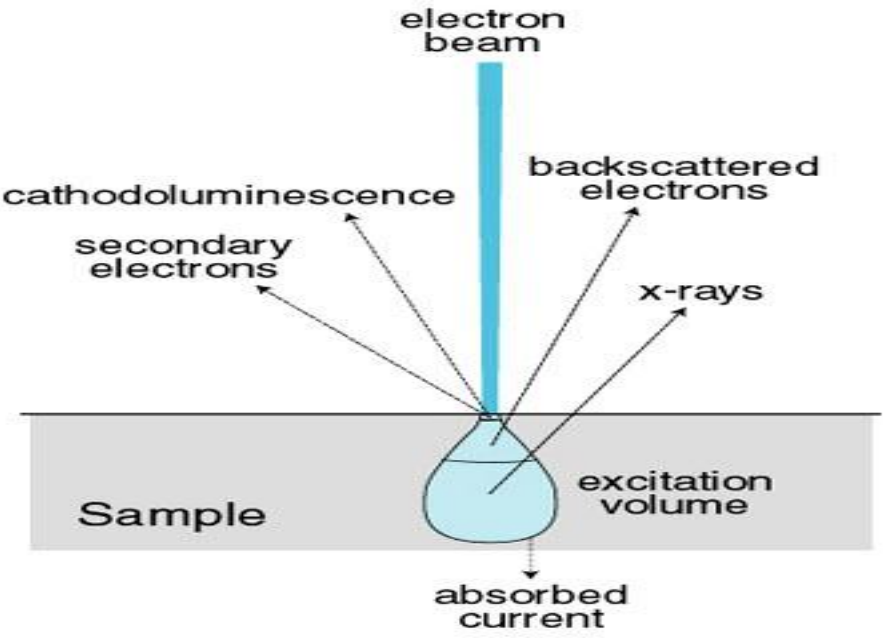

Figure 13: Various interaction process inside a sample.[71]

A typical SEM consists of electron gun, electron lenses, sample stage, detector for all signals of interest, display/data output devices. All Electron Microscopes utilize an electron source of some kind with the majority using a thermionic Gun, where electrons are thermionically emitted from a tungsten or lanthanum hexaboride (LaB_6) cathode and are accelerated towards an anode. In most applications, data are collected over a selected area of the surface of the sample, and a 2-dimensional image is generated that displays spatial variations in these properties. Areas ranging from approximately 1 cm to 5 microns in width can be imaged in a scanning mode using conventional SEM techniques (magnification ranging from 20X to approximately 30,000X, spatial resolution of

50 to 100 nm).[71] The SEM is also capable of performing analyses of selected point locations on the sample; this approach is especially useful in qualitatively or semi-quantitatively determining chemical compositions (using EDS), crystalline structure, and crystal orientations (using EBSD). (Scanning electron microscope)The design and function of the SEM is very similar to the EPMA and considerable overlap in capabilities exists between the two instruments. The figure below shows a typical SEM:

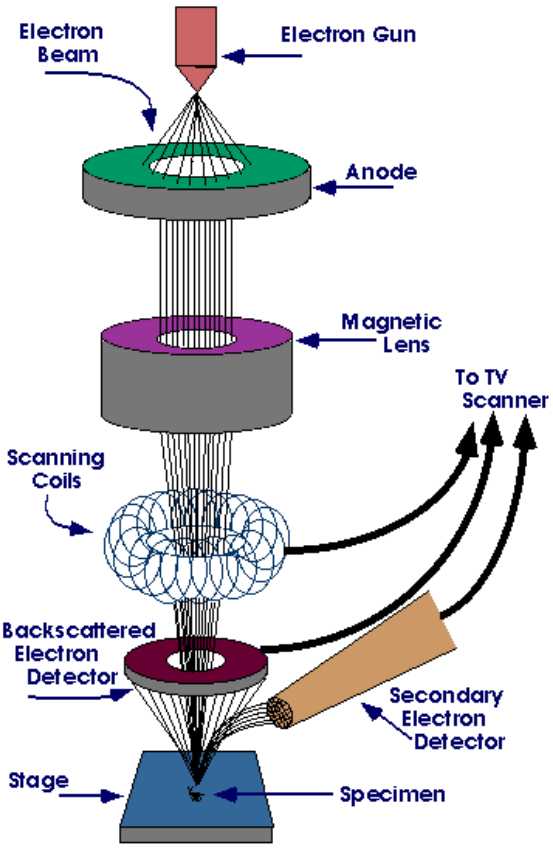

Figure 14: SEM (Scanning electron microscope).[72]

Detectors collect these X-rays, backscattered electrons, and secondary electrons and convert them into a signal that is sent to a screen similar to a television screen. This produces the final image. Because the SEM utilizes vacuum conditions and uses electrons to form an image, special preparations must be done to the sample. All water must be removed from the samples because the water would vaporize in the vacuum. All metals are conductive and require no preparation before being used. All non-metals need to be made conductive by covering the sample with a thin layer of conductive material. This is done by using a device called a "sputter coater." The sputter coater uses an electric field and argon gas. The sample is placed in a small chamber that is at a vacuum. Argon gas and an electric field cause an electron to be removed from the argon, making the atoms

positively charged. The argon ions then become attracted to a negatively charged gold foil. The argon ions knock gold atoms from the surface of the gold foil. These gold atoms fall and settle onto the surface of the sample producing a thin gold coating.

The Figure 15 shows the Hitachi-S-3700N SEM (Scanning electron microscope) available in Delhi Technological University, New Delhi.

Figure 15: Hitachi-S-3700N SEM (Scanning electron microscope)

3.5.2.1: Impedance Analyzers (LCR meter)

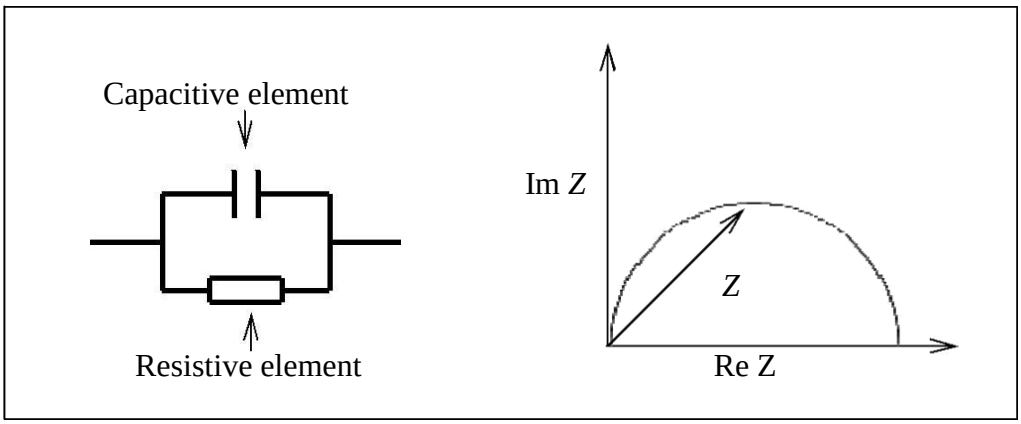

Figure 16(a): Simple equivalent circuit Figure 16(b): Nyquist plot with impedance vector.

Impedance is an important parameter used to characterize electronic circuits, components, and the materials used to make components. An impedance vector consists of a real part (resistance, R) and an imaginary part (reactance, X). Impedance can be expressed using the rectangular-coordinate form R+jX or in the polar form as a magnitude and phase angle: $|Z|\angle\theta$. An impedance vector consists of a real part (resistance, R) and an imaginary part (reactance, X). Impedance can be expressed using the

rectangular-coordinate form R+jX or in the polar form as a magnitude and phase angle: $|Z|\angle\theta$. The unit of impedance is the ohm (Ω), and admittance is the siemen). Impedance is a commonly used parameter and is especially useful for representing a series connection of resistance and reactance, Impedance is a commonly used parameter and is especially useful for representing a series connection of resistance and reactance, because it can be expressed simply as a sum, R and X. For a parallel connection, it is better to use admittance. This expression of impedance has real and imaginary parts. If the real part is plotted on an x-axis and the negative of the imaginary part on the y-axis, then a Nyquist plot is produced, as seen in Figure 16(b). Every point on this plot is an impedance at that given frequency. For a circuit with a resistor in parallel to a capacitive element Figure 16(a), then the Nyquist plot would appear like the one in Figure 16(b), where low frequency data is seen on the right side and high frequency data on the left side. The angle between the vector *Z* and the x-axis is known as the phase angle.

Figure 17: 4284A Precision LCR Meter

Generally, non-linear systems create harmonics of the excitation frequency which interfere with detection of the response signal $I(t)$. In EIS practice, this challenge is overcome by making the system pseudo-linear through use of a small AC voltage (1 to 10 mV). Good EIS measurements require steady state systems. In practice, this can be difficult as outside electrical noise, build up of chemicals, adsorption of impurities, temperature changes, could all interfere with the quality of measurement. Measurements across the frequency spectrum can sometimes last hours, so EIS systems are susceptible to error.

CHAPTER-4: RESULT AND DISCUSSION

4.1: Analysis of $Li_{1+x}Mn_{1-x}O_2$ (x=0.2)

The X-Ray diffraction patterns (Figure) were analyzed using X'Pert High Score Plus software. The X-Ray Diffraction image of the $Li_{1+x}Mn_{1-x}O_2$ (x=0.2) samples show that crystalline $Li_{1+x}Mn_{1-x}O_2$ (x=0.2) is formed. The XRD pattern matches with the PDF Reference Code: 01-086-0351. Hence, XRD pattern confirms the formation of $Li_{1+x}Mn_{1-x}O_2$ (x=0.2).

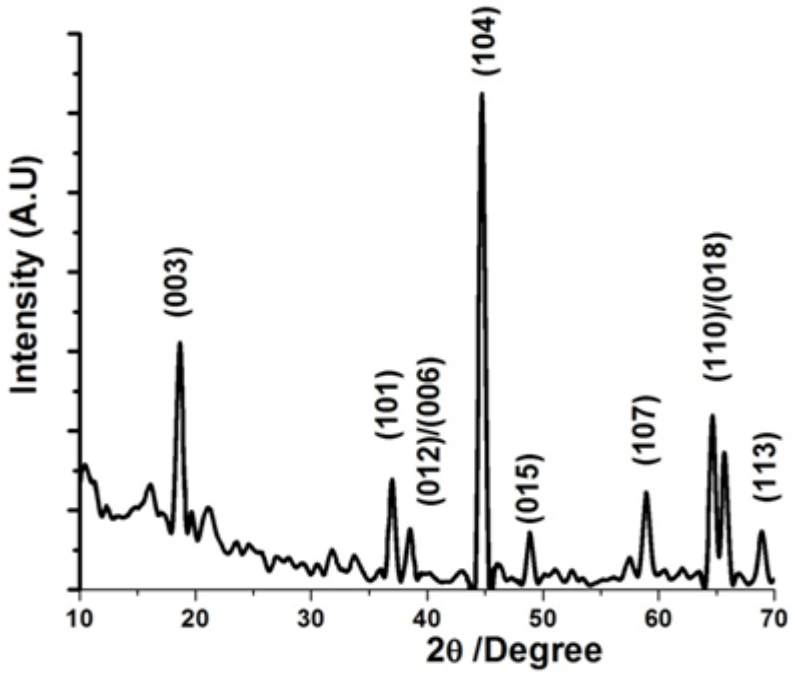

Figure 18: XRD Image of $Li_{1+x}Mn_{1-x}O_2$ (x=0.2) calcined at 750^0C for 12 hours in air

Crystallographic parameters

Crystal system:	Orthorhombic
Space group:	Pmnm
Space group number:	59
a (Å):	4.5780
b (Å):	5.7488

c (Å): 2.8054

Alpha (°): 90.0000

Beta (°): 90.0000

Gamma (°): 90.0000

Calculated density (g/cm^3): 4.22

Measured density (g/cm^3): 4.25

Volume of cell (10^6 pm^3): 73.83

The Crystallite sizes as calculated by the X'Pert High Score Software corresponding to the major peaks in the sample are as follows:

S. No.	B obs. [°2Th]	Peak pos. [°2Th]	d-Spacing size [Å]	Crystallite size [Å]
1.	0.712	18.670	4.7413	122
2.	0.259	36.994	2.4276	401
3.	0.583	44.829	2.0236	161
4.	0.194	48.843	1.8611	606
5.	.0453	59.009	1.5655	227
6.	0.583	64.577	1.4406	176
7.	0.842	65.613	1.4210	119
8.	0.324	68.915	1.3608	352

Table 3: Crystallite Size Calculation of $Li_{1+x}Mn_{1-x}O_2$ (x=0.2) calcined at 750^0C for 12 hours in air

The Average Crystallite Size of $Li1_{+x}Mn_{1-x}O_2$ (x=0.2) corresponding to eight major peaks is: **270.5 Å.**

The SEM micrograph of a gold coated $Li_{1+x}Mn_{1-x}O_2$ (x=0.2) sample was observed in Hitachi-S-3700N scanning electron microscope. The scanning electron microscope images of the $Li_{1+x}Mn_{1-x}O_2$ (x=0.2) calcined at 750^0C for 12 hours is shown in Figure 19(a), (b), (c) at different magnifications. Scanning electron microscope images of the $Li_{1+x}Mn_{1-x}O_2$ (x=0.2) showed magnified images of crystal grains. The average grain size was found to be in the range of 200-250 nm with uniform size distribution. It was proposed that the small particles sizes of even distribution is beneficial for better Li^+ diffusion and enhanced electronic transport at high current rates.[73,74]

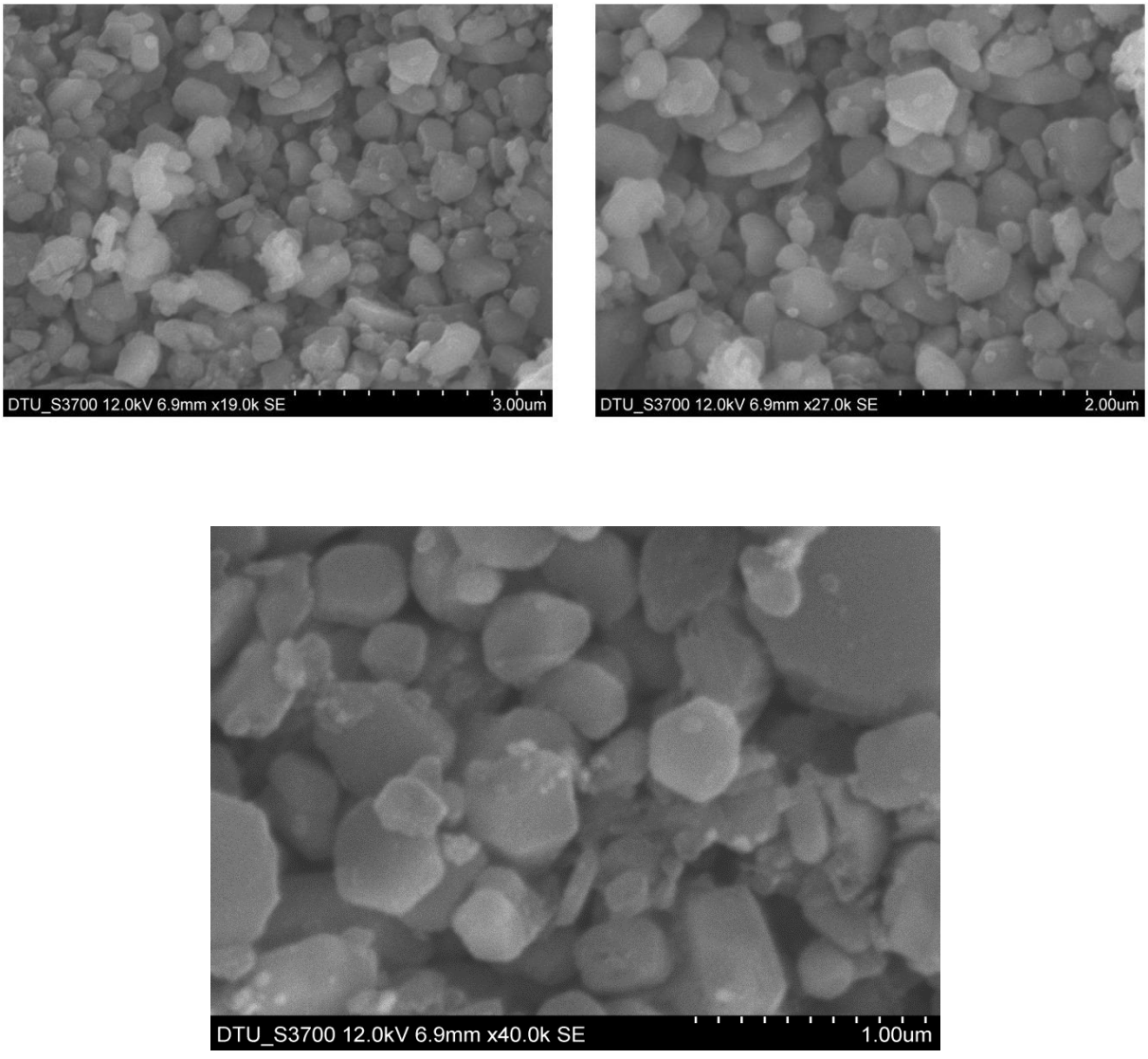

Figure 19: SEM image of $Li_{1+x}Mn_{1-x}O_2$ (x=0.2) calcined at 750^0C for 12 hours in air

The EDS data of $Li_{1+x}Mn_{1-x}O_2$ (x=0.2) showed that atomic percentage of manganese (Mn) and the atomic percentage of Oxygen (O) was almost two times the atomic percentage of manganese (Mn). Lithium being a very light element could not be detected in EDS analysis.

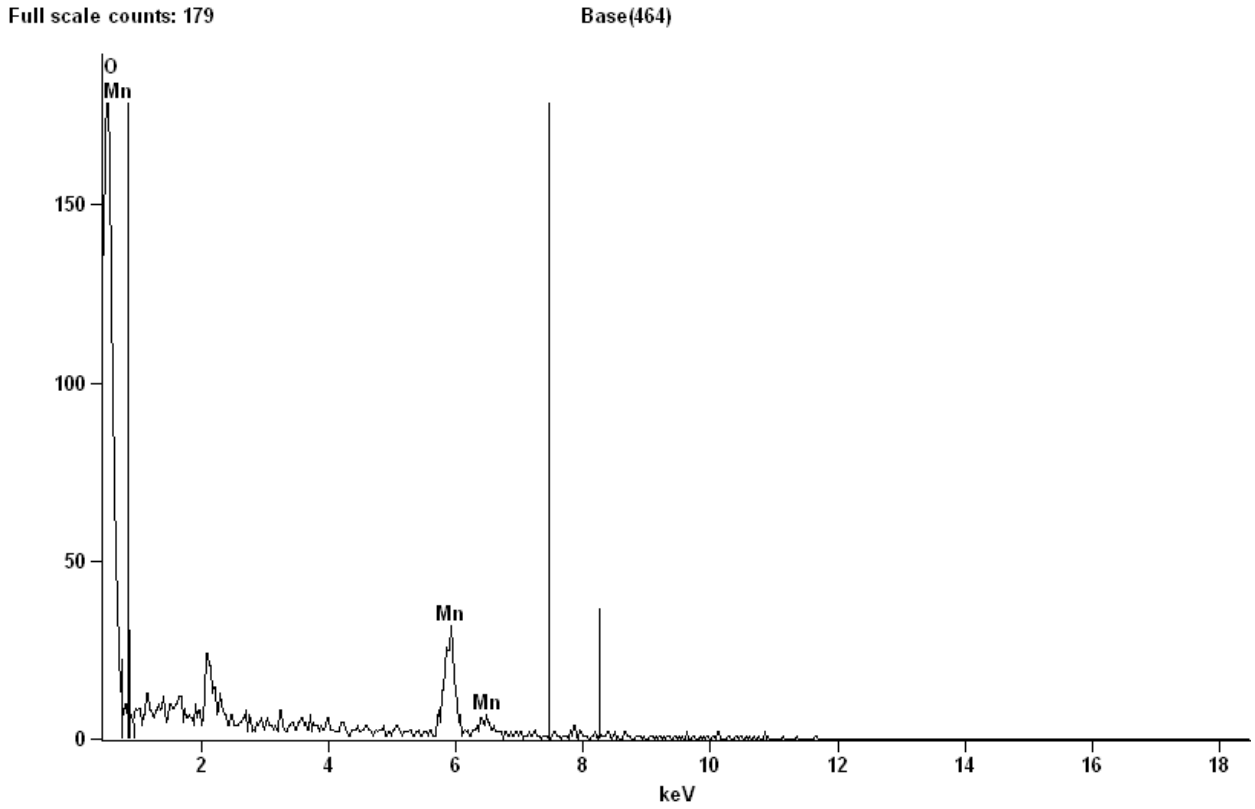

Figure 20: EDS Images of $Li_{1+x}Mn_{1-x}O_2$ (x=0.2) calcined at 750^0C for 12 hours in air

Element Line	Net Counts	Int. Cps/nA	Weight %	Weight % Error	Atom %	Atom % Error	Formula	Standard Name
O K	4130	---	65.43	+/- 1.90	86.67	+/- 2.52	O	
Mn K	522	---	34.57	+/- 2.58	13.33	+/- 1.00	Mn	
Mn L	1148	---	---	---	---	---		
Total			100.00		100.00			

Table 4: Weight Percentage of Element in $Li_{1+x}Mn_{1-x}O_2$ (x=0.2) calcined at 750^0C for 12 hours in air

Hence the EDS Analysis confirms the formation of $Li_{1+x}Mn_{1-x}O_2$ (x=0.2).

Impedance measurements were carried out by making pellets of calcined powder of diameter, 1.0 cm and thickness, 2.03 mm at room temperature using LCR METER (Agilent 4284A) in the frequency range of 20 Hz to 1 MHz The flat surface of the pellet was coated with gold and then heated at 400^0C to remove moisture. All the measurement has been done at biased voltage one volt.

The real and imaginary parts of the measured impedance values were plotted in a complex plane and shown in Figure 21(a). Bulk resistance (R) of the sample was calculated from the extrapolated semiconductor plot in the low frequency region on the X-axis. The electrical conductivity (σ) of the samples was calculated using the following relation:

$$\sigma = (1/R).(L/A) \qquad \ldots 13$$

Where L is the thickness of the sample and A is the area of the cylindrical sample.[75] the electrical conductivity (AC) of the material at the room temperature is of estimated of the order of 10^{-8} S/cm.

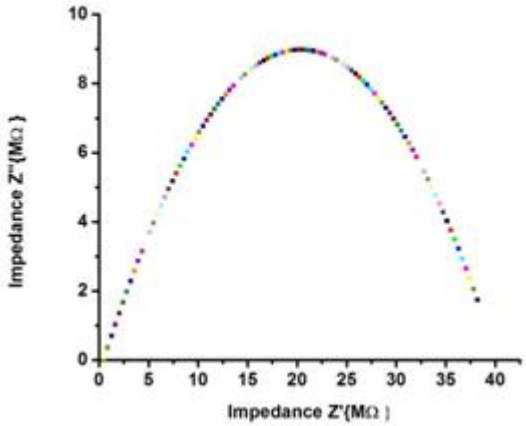

Figure 21(a): Variation of real and imaginary Parts of the measured Impedances

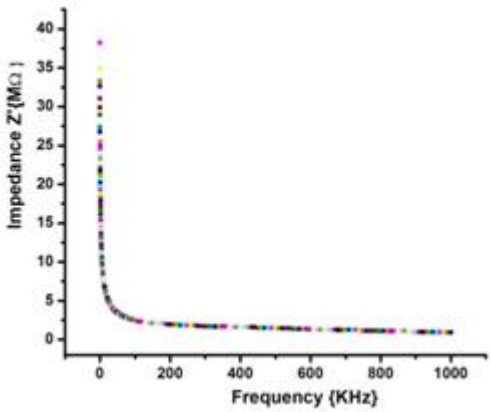

Figure 21(b): Variation of the real part of the Impedance with the frequency

Figure 21(b) shows the variation of the real part of the impedance with the frequency. It may be revealed that the impedance is higher at lower frequency range, which indicates that the molecules are in the polarization state at the lower frequencies and on increasing the frequencies the molecules in the compound attain relaxation state.

Figure 21(c) shows the variation of the Imaginary part of the impedance with the frequency. It may be revealed that the impedance is higher at lower frequency range, which indicates that the molecules are in the polarization state at the lower frequencies and on increasing the frequencies the molecules in the compound attain relaxation state.

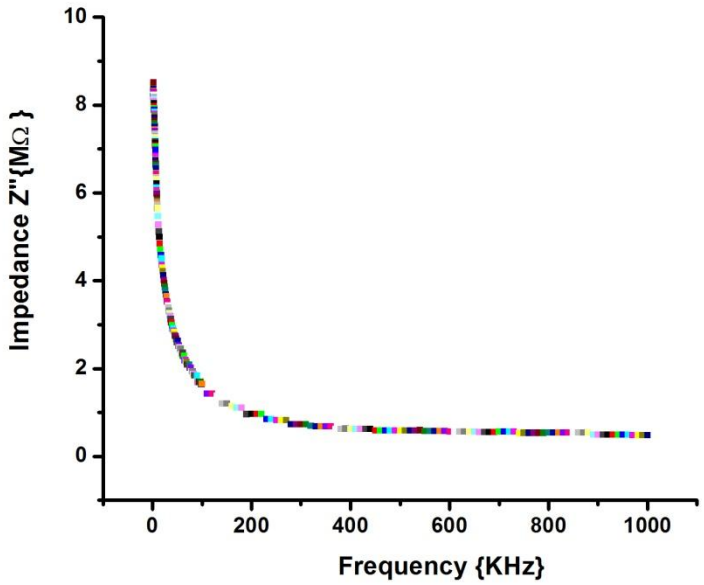

Figure 21(c): Variation of the Imaginary part of the Impedance with the frequency

It is also found that there is minor decrement in the impedance over the frequencies range of 20 Hz to 1 MHz shows that the material can remain in the polarization state over the frequency range.[76] hence, lithium intercalation into the host structure will be easy over the frequency range 20 Hz to 1 MHz.

4.2: Analysis of $Li_{1+x}\{Mn_{0.4}Ni_{0.4}Fe_{0.2}\}_{1-x}O_2$ (x=0.2) Synthesized in air atmosphere

The synthesized $Li_{1+x}\{Mn_{0.4}Ni_{0.4}Fe_{0.2}\}_{1-x}O_2$ (x=0.2) in air atmosphere powders were characterized using XRD for determination of crystal structure. Observed XRD pattern of $Li_{1+x}\{Mn_{0.4}Ni_{0.4}Fe_{0.2}\}_{1-x}O_2$ (x=0.2) is shown in Figure. The indexed peaks reveal the hexagonal α-$NaFeO_2$ type structure with a space group of R3m, indicating that a layer of lithium is substituted with a layer containing lithium, manganese, nickel and iron atoms.[77] Two small peaks observed between 20^0 and 30^0 indicating the additional supper lattices, due to the short range ordering of lithium, manganese, nickel and iron at the atomic site 3a resulting the existence of a layered structure with Li_2MnO_3.[78] The radius of Lithium-Ion, Li^+ (0.76Å) is greater than that of Nickel, Ni^{2+} (0.69 Å) and Mn^{4+} (0.53 Å, six fold coordination)[79] as proposed by Shannon et.al for the effect of ionic radii. As the radius of Li^+ is larger, the substitution of Li^+ for metal ions causes the increase in lattice parameters. Moreover, the c/a ratio of the sample is more than 4.90, it shows that the layered behaviour of synthesized sample. This is well known that with increasing c/a ratio beyond 4.90, the ordering of the layered structure increases and the crystal structure becomes more hexagonal.[80] the ratio of the intensity of peaks indexed at (003) to (004) i.e. I(0 0 3)/I(1 0 4) is of about 0.84,which is also agreement with the value given by the Ohzuku.[81] That is the indication of mixing between Ni^{2+} and Li^+ cations.[82]

The XRD pattern shows that crystalline $Li_{1+x}\{Mn_{0.4}Ni_{0.4}Fe_{0.2}\}_{1-x}O_2$ (x=0.2) was formed. The XRD peaks closely matched) with the peaks of $Li_{1+x}Mn_{1-x}O_2$ (x=0.2). This shows that doping of Nickel (Ni) and Iron (Fe) was successful along with crystalline grains and regions of different morphology having Iron (Fe), Nickel (Ni) and manganese (Mn).

Crystallographic parameters

Crystal system:	hexagonal
Space group:	R3m
a (Å):	2.895
c (Å):	14.330
c/a	4.95
I(0 0 3)/I(1 0 4)	1.42

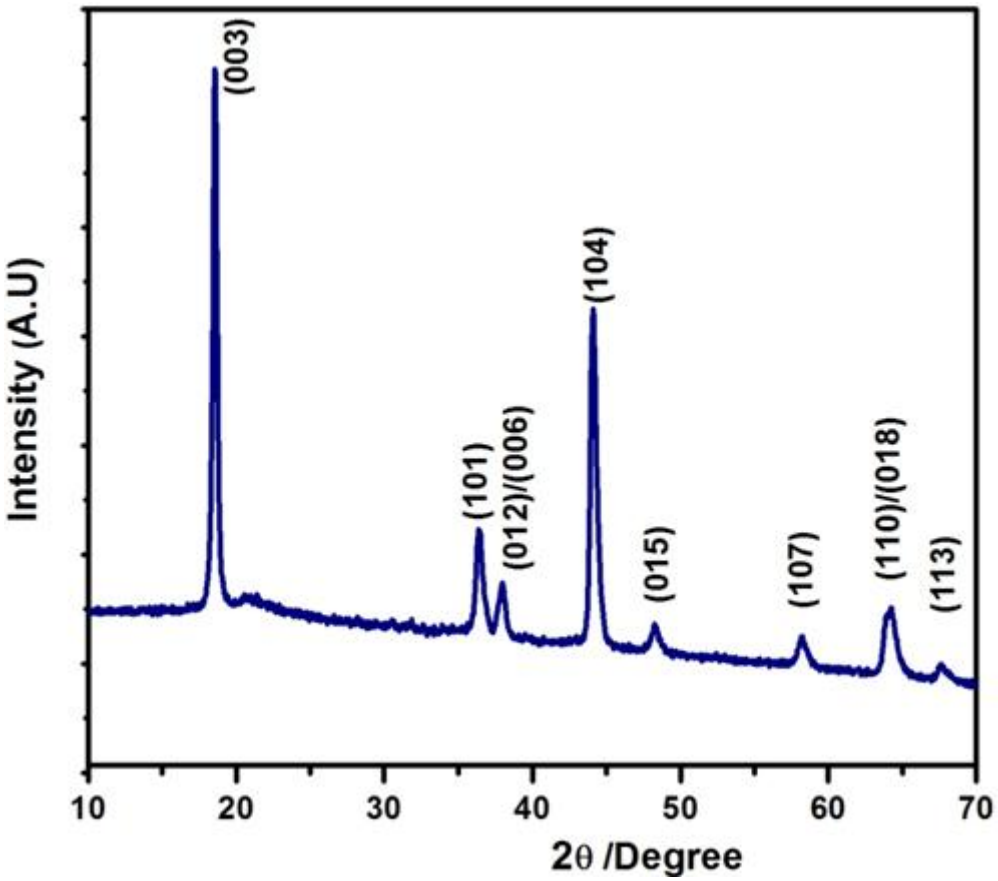

Figure 22: XRD Image of $Li_{1+x}\{Mn_{0.4}Ni_{0.4}Fe_{0.2}\}_{1-x}O_2$ (x=0.2) calcined at 750^0C for 14 hours in air

The Crystallite sizes as calculated by the X'Pert High Score Software corresponding to the major peaks in the sample are as follows:

S. No.	B obs. [°2Th]	Peak pos. [°2Th]	d-Spacing size [Å]	Crystallite size [Å]
1.	0.778	18.559	4.7768	111
2.	1.089	36.442	2.4650	180
3.	0.778	37.997	2.3672	215
4.	1.244	44.113	2.0519	173
5.	1.141	48.260	1.8835	180
6.	1.088	58.212	1.5834	188
7.	1.399	64.224	1.4492	170
8.	0.829	67.645	1.38387	123

Table 5: Crystallite Size Calculation of $Li_{1+x}\{Mn_{0.4}Ni_{0.4}Fe_{0.2}\}_{1-x}O_2$ (x=0.2) calcined at 750^0C for 14 hours in air

The Average Crystallite Size of $Li_{1+x}\{Mn_{0.4}Ni_{0.4}Fe_{0.2}\}_{1-x}O_2$ (x=0.2) corresponding to eight major peaks is: **167.5 Å.**

It is well-known that particle size and morphology of powders play a crucial role in determining the electrochemical performance of the material. The morphology and particle distribution of the layered powder prepared at 750^0C for 12 hours in air atmosphere is shown in Figure 23(a), (b), (c) at different magnification. From the figures, it is found that the uniformly distributed particles of prismatic shape and size lies in the range 100-150 nm are observed. It was proposed that the small particles size with even distribution is beneficial for better Li^+ diffusion and enhanced electronic transport at high current rates.[73,74]

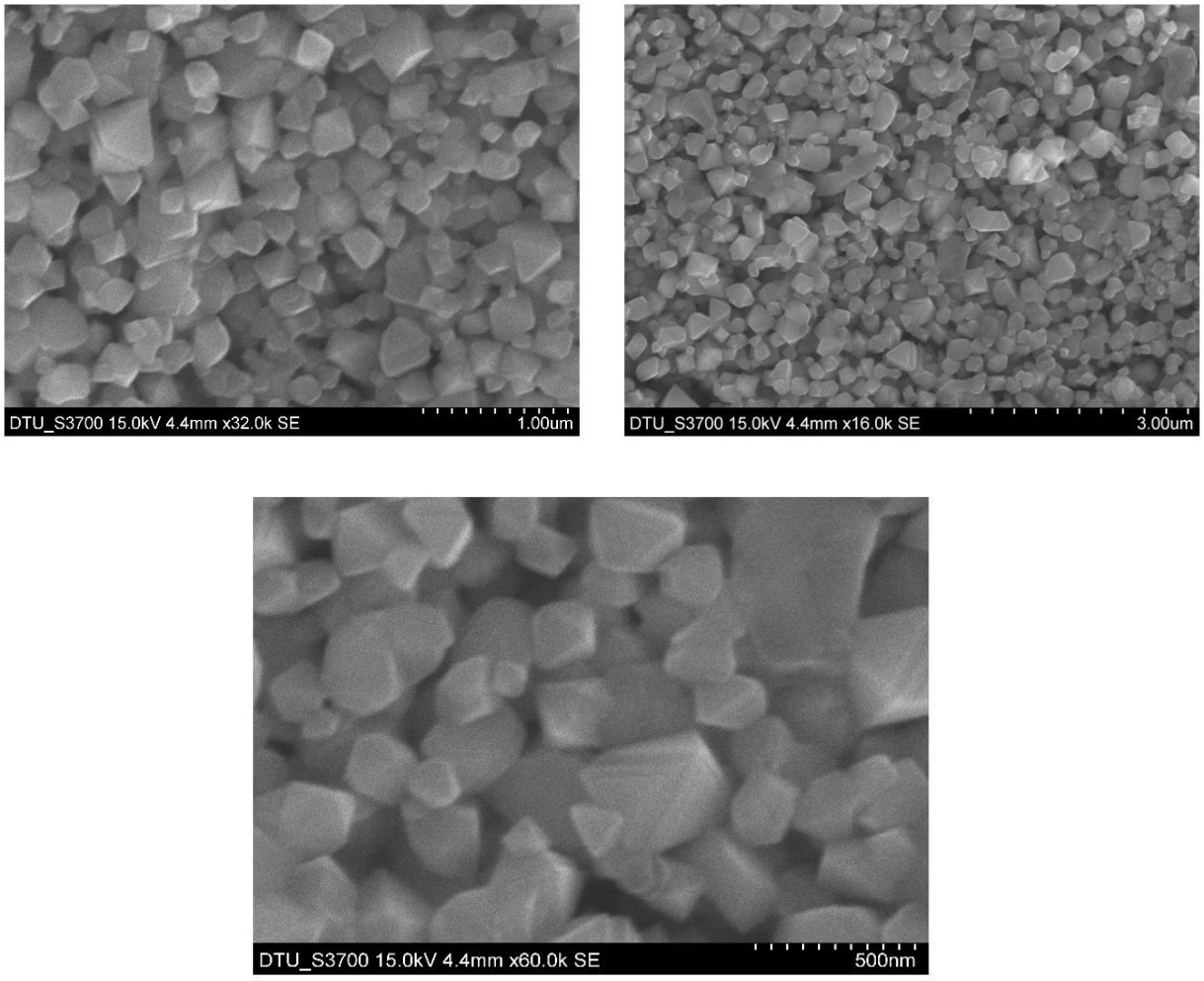

Figure 23: SEM Images of $Li_{1+x}\{Mn_{0.4}Ni_{0.4}Fe_{0.2}\}_{1-x}O_2$ (x=0.2) calcined at 750^0C for 14 hours in air

The EDS data of $Li_{1+x}\{Mn_{0.4}Ni_{0.4}Fe_{0.2}\}_{1-x}O_2$ (x=0.2) showed that Weight percentage of manganese (Mn), Nickel (Ni), and Iron (Fe). The Weight percentage of manganese (Mn) was almost equal to

Weight percentage of manganese (Ni) and almost equal to the two times of the weight percentage of Iron (Fe). Lithium being a very light element could not be detected in EDS analysis.

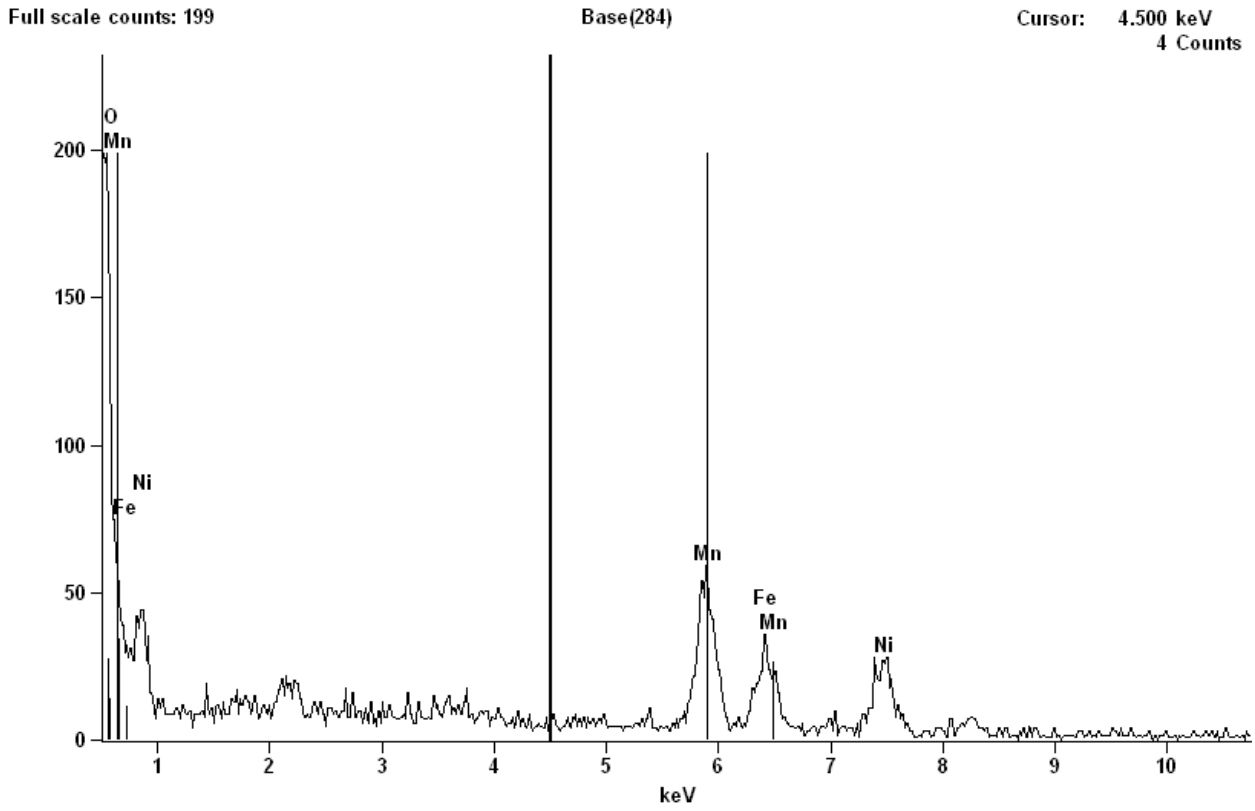

Figure 24: EDS Images of $Li_{1+x}\{Mn_{0.4}Ni_{0.4}Fe_{0.2}\}_{1-x}O_2$ (x=0.2) calcined at 750^0C for 14 hours in air

Table 6 shows the Weight Percentage of Element in $Li_{1+x}\{Mn_{0.4}Ni_{0.4}Fe_{0.2}\}_{1-x}O_2$ (x=0.2) synthesized in air.

Element Line	Net Counts	Int. Cps/nA	Weight %	Weight % Error	Atom %	Atom % Error	Formula	Standard Name
O K	3697	---	31.83	+/- 0.65	62.30	+/- 1.26	O	
Mn K	950	---	27.32	+/- 1.67	15.57	+/- 0.95	Mn	
Mn L	0	---	---	---	---	---		
Fe K	397	---	12.65	+/- 1.47	7.09	+/- 0.82	Fe	
Fe L	1622	---	---	---	---	---		
Ni K	529	---	28.20	+/- 3.57	15.04	+/- 1.90	Ni	
Ni L	665	---	---	---	---	---		
Total			100.00		100.00			

Table 6: Weight Percentage of Element in $Li_{1+x}\{Mn_{0.4}Ni_{0.4}Fe_{0.2}\}_{1-x}O_2$ (x=0.2) calcined at 750^0C for 14 hours in air

Hence the EDS Analysis confirms the formation of $Li_{1+x}\{Mn_{0.4}Ni_{0.4}Fe_{0.2}\}_{1-x}O_2$ (x=0.2).

Impedance measurements were carried out by making pellets of calcined powder of diameter, 1.0 cm and thickness, 1.98 mm at room temperature using LCR METER (Agilent 4284A) in the frequency range of 20 Hz to 1 MHz. The flat surface of the pellet was coated with gold and then heated at 400^0C to remove moisture. All the measurement has been done at biased voltage one volt.

The real and imaginary parts of the measured impedance values were plotted in a complex plane and shown in Figure 25(a). Bulk resistance (R) of the sample was calculated from the extrapolated semiconductor plot in the low frequency region on the X-axis. The electrical conductivity (σ) of the samples was calculated using the equation 13.

the electrical conductivity (AC) of the material at the room temperature is of estimated of the order of 10^{-6} S/cm.

Figure 25(b) shows the variation of the real part of the impedance with the frequency. It may be revealed that the impedance is higher at lower frequency range, which indicates that the molecules are in the polarization state at the lower frequencies and on increasing the frequencies the molecules in the compound attain relaxation state.

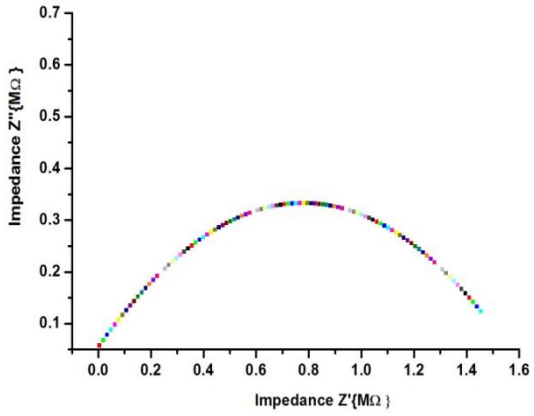

Figure 25(a): Variation of real and imaginary Parts of the measured impedances

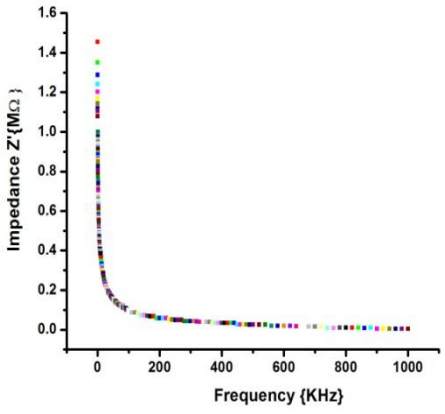

Figure 25(b): Variation of the real part of the impedance with the frequency

Figure 25(c) shows the variation of the Imaginary part of the impedance with the frequency. It may be revealed that the impedance is higher at lower frequency range, which indicates that the molecules are in the polarization state at the lower frequencies and on increasing the frequencies the molecules in the compound attain relaxation state.

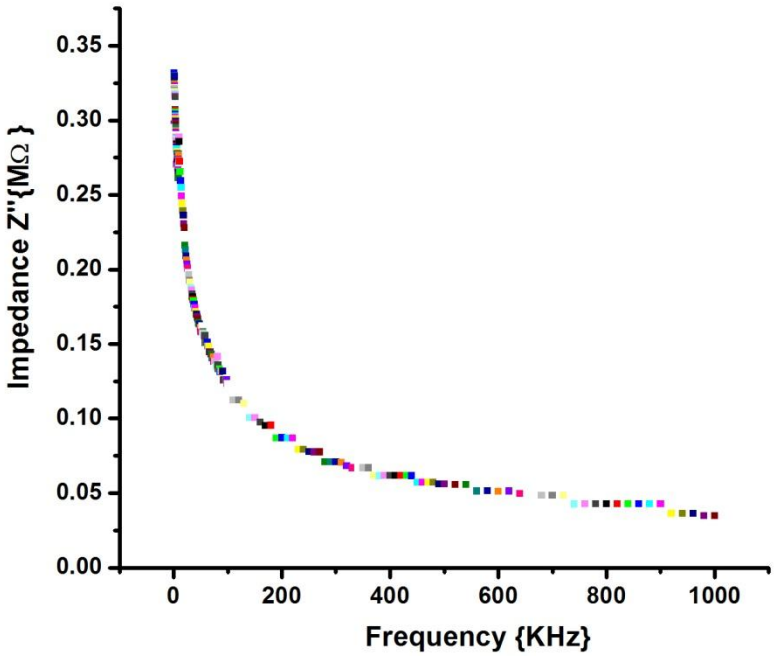

Figure 25(c): Variation of the Imaginary part of the Impedance with the frequency

It is also found that there is minor decrement in the impedance over the frequencies range of 20 Hz to 1 MHz shows that the material can remain in the polarization state over the frequency range.[76] Hence, lithium intercalation into the host structure will be easy over the frequency range 20 Hz to 1 MHz.

4.3: Analysis of $Li_{1+x}\{Mn_{0.4}Ni_{0.4}Fe_{0.2}\}_{1-x}O_2$ (x=0.2) in inert atmosphere

The synthesized $Li_{1+x}\{Mn_{0.4}Ni_{0.4}Fe_{0.2}\}_{1-x}O_2$ (x=0.2) in inert Atmosphere powders were characterized using XRD for determination of crystal structure. Observed XRD pattern of $Li_{1+x}\{Mn_{0.4}Ni_{0.4}Fe_{0.2}\}_{1-x}O_2$ (x=0.2) is shown in Figure. The indexed peaks reveal the hexagonal α-$NaFeO_2$ type structure with a space group of R3m, indicating that a layer of lithium is substituted with a layer containing lithium, manganese, nickel and iron atoms.[77] Two small peaks observed between 20^0 and 30^0 indicating the additional supper lattices, due to the short range ordering of lithium, manganese, nickel and iron at the atomic site 3a resulting the existence of a layered structure with Li_2MnO_3.[78] The radius of Lithium-Ion, Li^+ (0.76Å) is greater than that of Nickel, Ni^{2+} (0.69 Å) and Mn^{4+} (0.53 Å, six fold coordination).[79] as proposed by Shannon et.al for the effect of ionic radii. As the radius of Li^+ is larger, the substitution of Li^+ for metal ions causes the increase in lattice parameters. Moreover, the c/a ratio of the sample is more than 4.90, it shows that the layered behaviour of synthesized sample. This is well known that with increasing c/a ratio beyond 4.90, the ordering of the layered structure increases and the crystal structure becomes more hexagonal.[80] the ratio of the intensity of peaks indexed at (003) to (004) i.e. I(0 0 3)/I(1 0 4) is of about 0.84,which is also agreement with the value given by the Ohzuku.[81] That is the indication of mixing between Ni^{2+} and Li^+ cations.[82]

The XRD pattern shows that crystalline $Li_{1+x}\{Mn_{0.4}Ni_{0.4}Fe_{0.2}\}_{1-x}O_2$ (x=0.2) was formed. The XRD peaks closely matched) with the peaks of $Li_{1+x}Mn_{1-x}O_2$ (x=0.2). This shows that doping of Nickel (Ni) and Iron (Fe) was successful. Along with crystalline grains, regions of different morphology having Iron (Fe), Nickel (Ni) and manganese (Mn).

Crystallographic parameters

Crystal system:	hexagonal
Space group:	R3m
a (Å):	2.895
c (Å):	14.278
c/a	4.93
I(0 0 3)/I(1 0 4)	1.34

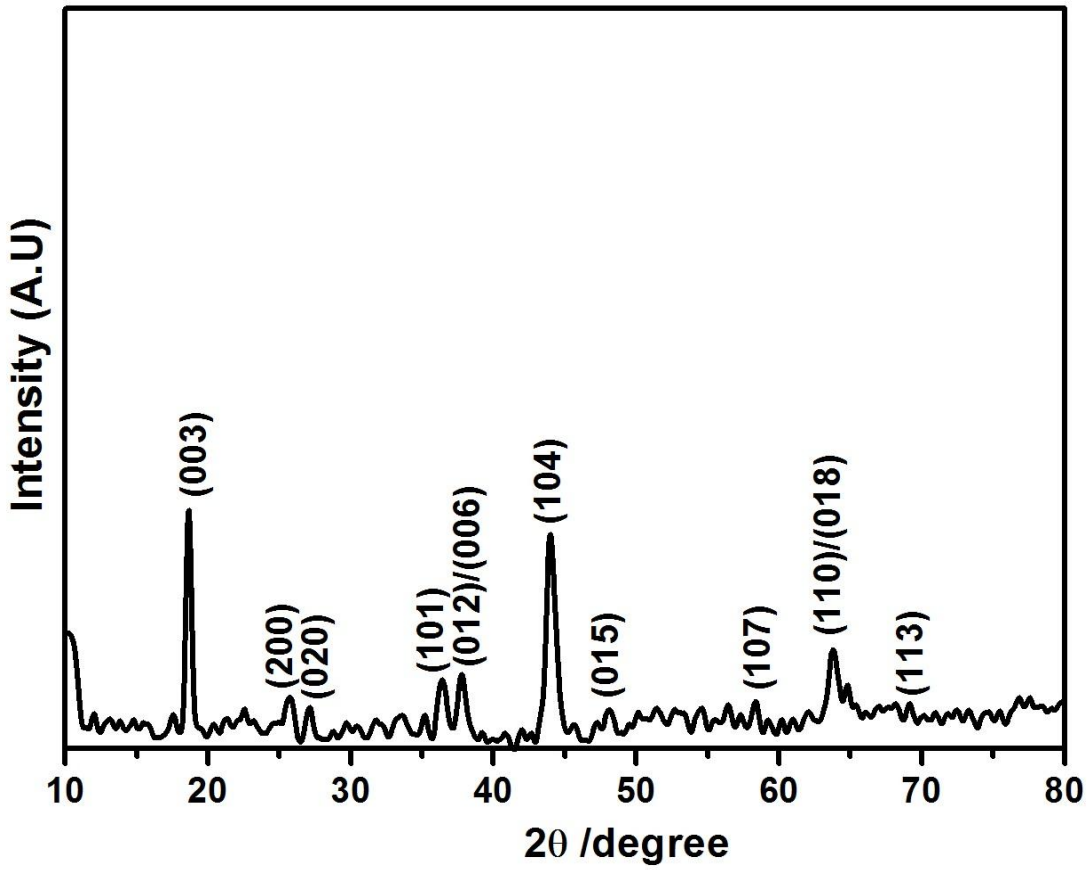

Figure 26: XRD Image of $Li_{1+x}\{Mn_{0.4}Ni_{0.4}Fe_{0.2}\}_{1-x}O_2$ (x=0.2) calcined at 750^0C for 12 hours in inert atmosphere

The Crystallite sizes as calculated by the X'Pert High Score Software corresponding to the major peaks in the sample are as follows:

S. No.	B obs. [°2Th]	Peak pos. [°2Th]	d-Spacing size [Å]	Crystallite size [Å]
1.	0.778	18.559	4.7968	131
2.	1.089	36.442	2.4850	190
3.	0.778	37.997	2.3872	235
4.	1.244	44.113	2.1519	193
5.	1.141	48.260	1.9835	240
6.	1.088	58.212	1.6834	208
7.	1.399	64.224	1.8492	220
8.	0.829	67.645	1.48387	223

Table 7 Crystallite Size Calculation of $Li_{1+x}\{Mn_{0.4}Ni_{0.4}Fe_{0.2}\}_{1-x}O_2$ (x=0.2) calcined at 750^0C for 12 hrs in inert atmosphere

The Average Crystallite Size of $Li_{1+x}\{Mn_{0.4}Ni_{0.4}Fe_{0.2}\}_{1-x}O_2$ (x=0.2) corresponding to eight major peaks is: **205 Å.**

The morphology and particle size of the layered powder prepared at 750^0C for 12 hours in inert atmosphere is shown in Figure 27(a), (b), (c) at different magnification.

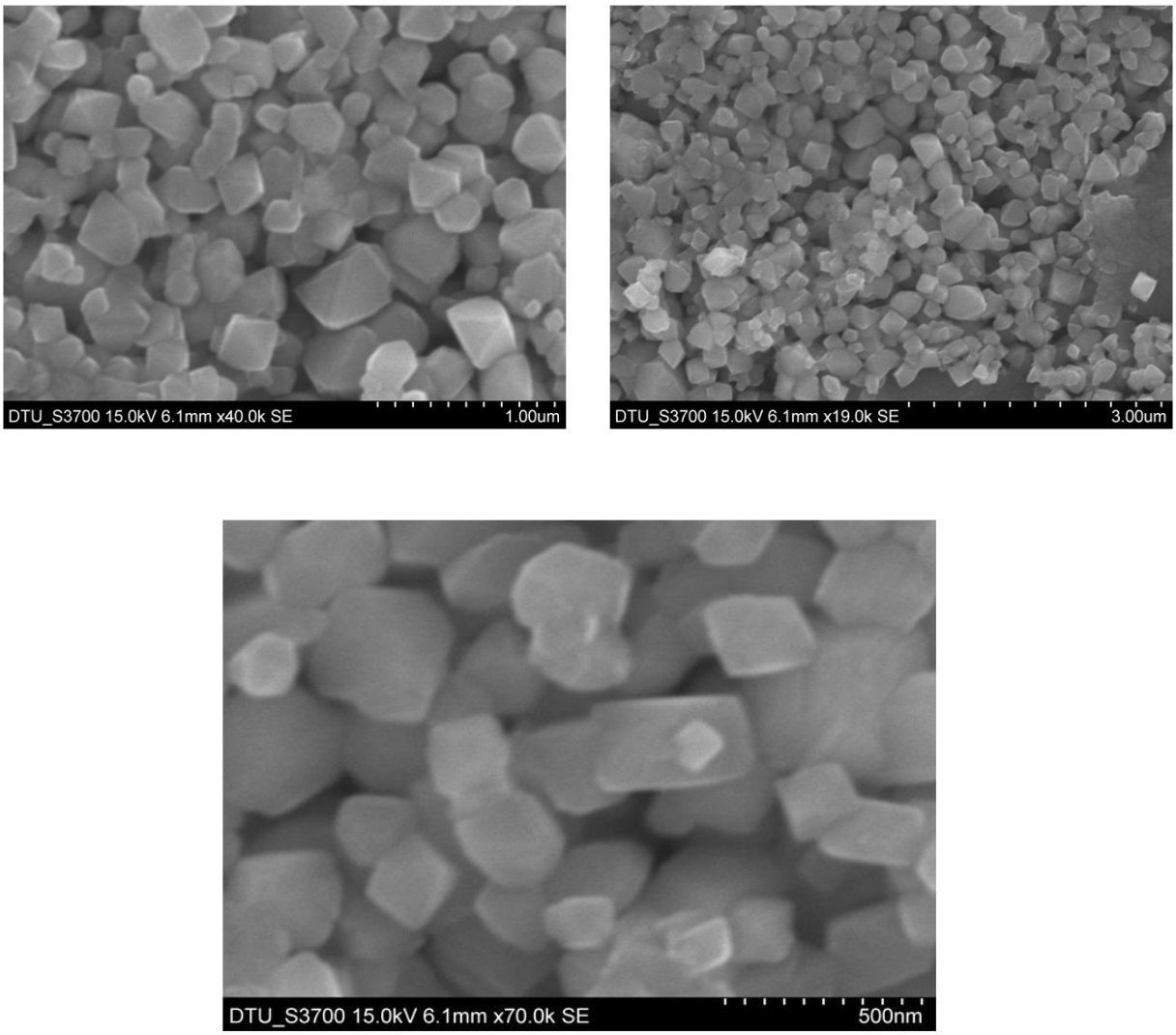

Figure 27: SEM Images of $Li_{1+x}\{Mn_{0.4}Ni_{0.4}Fe_{0.2}\}_{1-x}O_2$ (x=0.2) calcined at 750^0C for 12 hours in inert atmosphere

From the figures, it is found that the uniformly distributed particles of prismatic shape and size lies in the 100-150nm are observed. Here it seems that no significant change observed on changing the environment during calcinations.

The EDS data of $Li_{1+x}\{Mn_{0.4}Ni_{0.4}Fe_{0.2}\}_{1-x}O_2$ (x=0.2) showed that Weight percentage of manganese (Mn), Nickel (Ni), and Iron (Fe). The Weight percentage of manganese (Mn) was almost equal to

Weight percentage of manganese (Ni) and almost equal to the two times of the weight percentage of Iron (Fe). Lithium being a very light element could not be detected in EDS analysis.

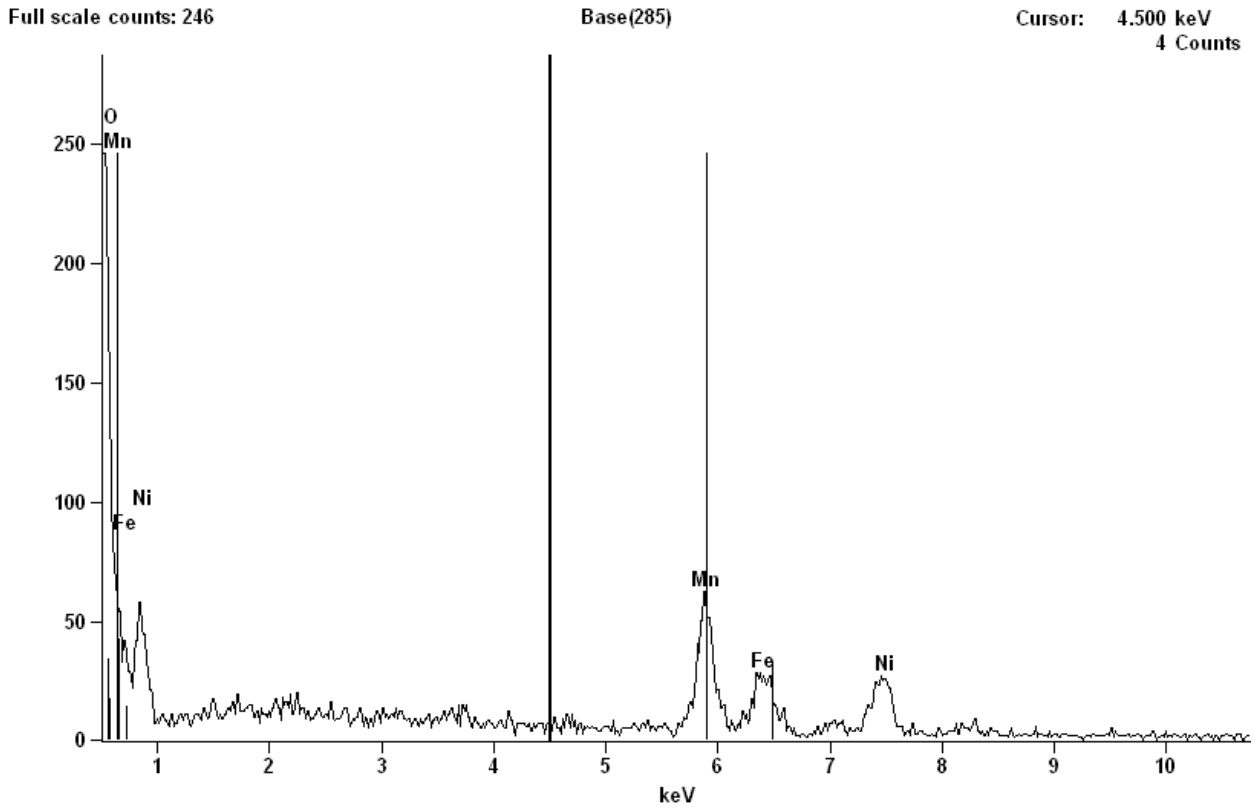

Figure 28: EDS Images of $Li_{1+x}\{Mn_{0.4}Ni_{0.4}Fe_{0.2}\}_{1-x}O_2$ (x=0.2) calcined at 750^0C for 12 hours in inert atmosphere

Element Line	Net Counts	Int. Cps/nA	Weight %	Weight % Error	Atom %	Atom % Error	Formula	Standard Name
O K	3969	---	34.77	+/- 0.66	65.33	+/- 1.23	O	
Mn K	899	---	26.79	+/- 1.64	14.66	+/- 0.90	Mn	
Mn L	0	---	---	---	---	---		
Fe K	380	---	12.54	+/- 1.48	6.75	+/- 0.80	Fe	
Fe L	1573	---	---	---	---	---		
Ni K	470	---	25.90	+/- 2.42	13.26	+/- 1.24	Ni	
Ni L	741	---	---	---	---	---		
Total			100.00		100.00			

Table 8: Weight Percentage of Element in $Li_{1+x}\{Mn_{0.4}Ni_{0.4}Fe_{0.2}\}_{1-x}O_2$ (x=0.2) calcined at 750^0C for 12 hours in inert

Hence the EDS Analysis confirms the formation of $Li_{1+x}\{Mn_{0.4}Ni_{0.4}Fe_{0.2}\}_{1-x}O_2$ (x=0.2) in inert atmosphere.

Impedance measurements were carried out by making pellets of calcined powder of diameter, 1.0 cm and thickness, 1.88 mm at room temperature using LCR METER (Agilent 4284A) in the frequency

range of 20 Hz to 1 MHz The flat surface of the pellet was coated with gold and then heated at 400^0C to remove moisture. All the measurement has been done at biased voltage one volt.

The real and imaginary parts of the measured impedance values were plotted in a complex plane and shown in Figure 29(a). Bulk resistance (R) of the sample was calculated from the extrapolated semiconductor plot in the low frequency region on the X-axis. The electrical conductivity (σ) of the samples was calculated using the equation 13.

The electrical conductivity (AC) of the material at the room temperature is of estimated of the order of 10^{-6} S/cm. it seem that there is no change in conductivity also as the change of air to inert atmosphere.

Figure 29(b) shows the variation of the real part of the impedance with the frequency. It may be revealed that the impedance is higher at lower frequency range, which indicates that the molecules are in the polarization state at the lower frequencies and on increasing the frequencies the molecules in the compound attain relaxation state.

Figure 29(c) shows the variation of the Imaginary part of the impedance with the frequency. It may be revealed that the impedance is higher at lower frequency range, which indicates that the molecules are in the polarization state at the lower frequencies and on increasing the frequencies the molecules in the compound attain relaxation state.

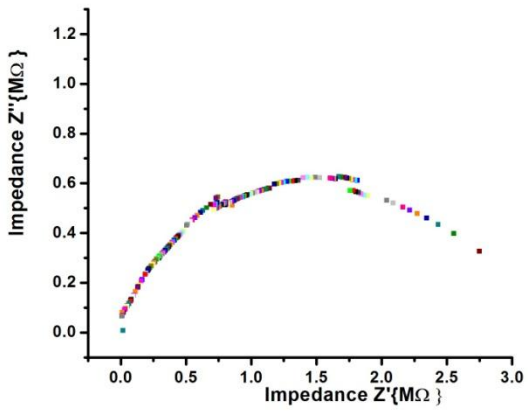

Figure 29(a): Variation of real and imaginary Parts of the measured impedances

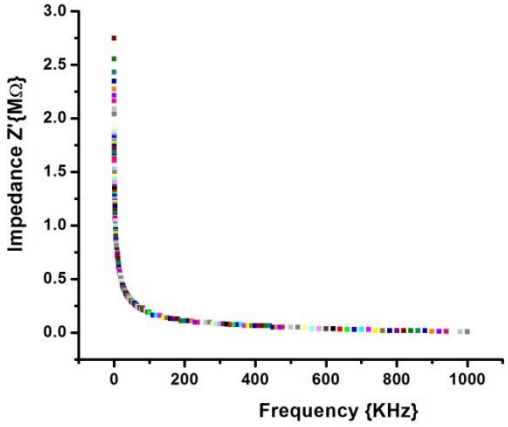

Figure 29(b): Variation of the real part of the impedance with the frequency

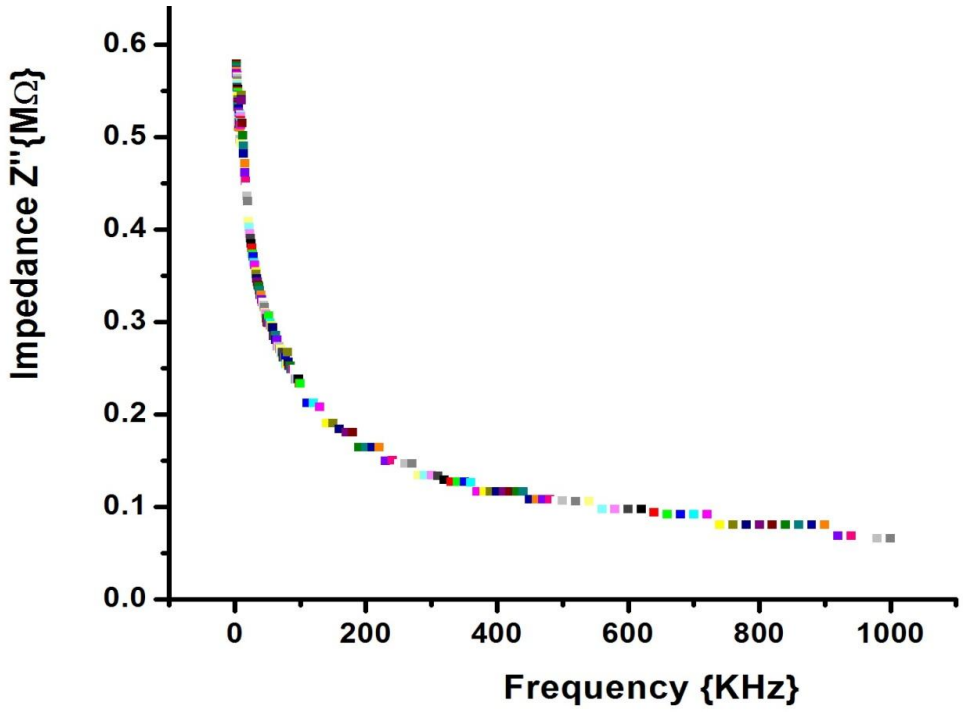

Figure 29(c): Variation of the Imaginary part of the Impedance with the frequency

It is also found that there is minor decrement in the impedance over the frequencies range of 20 Hz to 1 MHz shows that the material can remain in the polarization state over the frequency range.[75] Hence, lithium intercalation into the host structure will be easy over the frequency range 20 Hz to 1 MHz.

CHAPTER 5: SUMMARY AND CONCLUSIONS

This research work has explored a sol-gel Route for synthesis of alternative nanostructure cathode materials for lithium-ion batteries. As the nanostructural cathode materials for lithium-ion batteries may useful to increase the electronic transport at high current rates with uniformly distribution of particles and electrode/electrolyte contact surface and shorten the lithium diffusion length.

A well crystalline layered $Li_{1+x}Mn_{1-x}O_2$ (x=0.2) cathode materials using a chelating agent as citric acid were successfully synthesized through the conventional sol-gel route. The phase formation of layered $Li_{1+x}Mn_{1-x}O_2$ (x=0.2) with crystal system Orthorhombic, space group Pmnm, confirmed by XRD. The XRD results revealed that the use of a high concentration of chelating agent improved the crystalline nature of the layered compound Scanning electron microscope (SEM) analysis reveals the existence of the uniformly distributed, prismatic shape of particles in the range of 200-250 nm. AC conductivity of the material at the room temperature is found of the order of 10^{-8} S/cm, in the semiconducting range. However, overall electrochemical performance will show the potentially of the prepared materials over other cathode materials, which has yet to the increase in conductivity.

Another layered $Li_{1+x}\{Mn_{0.4}Ni_{0.4}Fe_{0.2}\}_{1-x}O_2$ (x=0.2) cathode materials on substitution of Mn by Fe and Ni using the a chelating agent as citric acid, were successfully synthesized in both air and Inert Atmosphere through the conventional sol–gel route. The layered materials containing iron could be one of the promising materials for Lithium-ion batteries at low cost and eco-friendly energy resource at large scale. The phase formation of layered $Li_{1+x}\{Mn_{0.4}Ni_{0.4}Fe_{0.2}\}_{1-x}O_2$ (x=0.2) with R3m space group has been confirmed by XRD. The XRD results revealed that the use of a high concentration of chelating agent improved the crystalline nature of the layered compound Scanning electron microscope (SEM) analysis reveals the existence of the uniformly distributed, prismatic shape of particles in the range of 100-150 nm. AC conductivity of the material at the room temperature is found of the order of 10^{-6} S/cm, in the semiconducting range. While is 100 times more than the parent $Li_{1+x}Mn_{1-x}O_2$ (x=0.2). However, overall electrochemical performance will show the potentially of the prepared materials over other cathode materials, which has yet to be performed. These experimental results suggest that citric acid mediated $Li_{1+x}\{Mn_{0.4}Ni_{0.4}Fe_{0.2}\}_{1-x}O_2$ (x=0.2) is an "eco-friendly" candidate for next generation cathode materials for Lithium-ion batteries.

On substitution of Mn by Fe and Ni the particle shape is changed and the particle size reduces significantly an observed from SEM micrograph. Also the AC conductivity of Fe and Ni substituted

sample increase approximately 100 times. However, no significantly change is observed on changing the atmosphere from air to inert.

Future Work

The electrochemical analysis of crystalline layered cathode material $Li_{1+x}Mn_{1-x}O_{2,}$ (x=0.2) and $Li_{1+x}\{Mn_{0.4}Ni_{0.4}Fe_{0.2}\}_{1-x}O_2$ (x=0.2) in air and inert atmosphere yet to be performed and it will lead to the best alternative cathode material for Lithium-ion batteries and compatibility with carbon band anode materials.

REFERENCES

[1]. Hall P. J.; Bain E. J.; "Energy-storage technologies and electricity generation." *Energy Policy*, **2008**, *36*, 4352-4355.

[2]. Arico A. S.; Bruce P.; Scrosati B.; Tarascon J.M.; van Schalkwijk W.; "Nanostructured materials for advanced energy conversion and storage devices." *Nat. Mater*., **2005**, *4*, 366-377.

[3]. Armand M.; Tarascon J.M.; "Issue and challenges facing rechargeable lithium batteries." *Nature*, **2001**, *414*, 359-367.

[4]. Armand M.; Tarascon J. M.; "Building better batteries." Nature, **2008**, *451*, 652-657.

[5]. Bashash S.; Moura S. J.; Forman J. C.; Fathy H. K.; "Plug-in hybrid electric vehicle charge pattern optimization for energy cost and battery longevity." *J. Power Sources.* **2011**, *196*, 541-549.

[6]. Wadia C.; Albertus P.; Srinivasan V.; "Resource constraints on the battery energy storage potential for grid and transportation applications." *J. Power Sources,* **2011**, *196*, 1593-1598.

[7]. Tarascon J. M.; Armand M.; "Issues and challenges facing rechargeable lithium batteries." *Nature,* **2001**, *414*, 359-367.

[8]. Etacheri V.; Marom R.; Elazari R.; Salitra G.; Aurbach D.; "Challenges in the development of advanced Li-ion batteries: a review." *Energy Environ. Sci.*, **2011**, *4*, 3243-3262.

[9]. Bruce P. G.; Freunberger S. A.; Hardwic, L. J.; Tarascon J. M.; "Li-O_2 and Li-S batteries with high energy storage." *Nat. Mater.*, **2012**, *11*, 19-29.

[10]. Toprakci O.; Toprakci H.; Ji L.; Zhang X.; "Fabrication and Electrochemical Characteristics of $LiFePO_4$ Powders for Lithium–Ion Batteries." *J. Kona Powder and Particle,* **2010**, *28*, 50-72.

[11]. Girishkumar G.; McCloskey B.; Luntz A. C.; Swanson S.; Wilcke W.; "Lithium - air Battery promise and challenges." *J. Phys. Chem. Lett.*, **2010**, *1*, 2193-2203.

[12]. Chen J.; "Recent Progress in Advanced Materials for Lithium-Ion Batteries." *Materials.*, **2013**, *6*, 156-183.

[13]. Scrosati B.; "History of lithium batteries." *J. Solid State Electrochem*, **2011**, *15*, 1623-1630.

[14]. Gamble F. R.; Osiecki J. H.; Cais M.; Pisharod R.; "Intercalation complexes of lewis bases and layered sulfides - large class of new superconductors." *Science,* **1971**, *174*, 493-497.

[15]. Whittingham M. S.; "Hydrated intercalation complexes of layered disulfides." *Mater. Res. Bull.*, **1974**, *9*, 1681-1690.

[16]. Whittingham M. S.; "Electrointercalation in transition-metal disulfides." *J. Chem. Soc., Chem. Commun.*, **1974**, *9*, 328-329.

[17]. Whittingham M. S.; "Electrical energy-storage and intercalation chemistry." *Science*, **1976**, *192*, 1126-1127.

[18]. Thompson A. H.; "Electron-electron scattering in TiS_2." *Phys. Rev. Lett.*, **1975**, *35*, 1786-1789.

[19]. Whittingham M. S.; "Role of ternary phases in cathode reactions." *J. Electrochem. Soc.*, **1976**, *123*, 315-320.

[20]. Whittingham M. S.; "Lithium batteries and cathode materials." *Chem. Rev.*, **2004**, *104*, 4271-4301.

[21]. Walk C. R.; Gore J. S.; "Li-V_2O_5 secondary cell." *J. Electrochem. Soc.*, **1975**, *122*, C68-C68.

[22]. Delmas C.; Cognacauradou H.; Cocciantelli J. M.; Menetrier M.; Doumerc J. P.; "The $Li_xV_2O_5$ system - an overview of the structure modifications induced by the lithium intercalation." *Solid State Ionics*, **1994**, *69*, 257-264.

[23]. Dickens P. G.; French S. J.; Hight A. T.; Pye M. F.; "Phase-relationships in the ambient-temperature $Li_xV_2O_5$ system ($0.1<x<1.0$)." *Mater. Res. Bull.*, **1979**, *14*, 1295-1299.

[24]. Mizushima K.; Jones P. C.; Wiseman P. J.; Goodenough J. B.; "Li_xCoO_2 ($0<x<.1$): a new cathode material for batteries of high-energy density." *Mater. Res. Bull.*, **1980**, *15*, 783-789.

[25]. Amatucci G. G.; Tarascon J. M.; Klein L. C.; "CoO_2, the end member of the Li_xCoO_2 solid solution." *J. Electrochem. Soc.*, **1996**, *143*, 1114-1123.

[26]. Yazami R.; Touzain P.; "A reversible graphite-lithium negative electrode for electrochemical generators." *J. Power Sources*, **1983**, *9*, 365-371.

[27]. Ozawa K.; "Lithium-ion rechargeable batteries with $LiCoO_2$ and carbon electrodes: the $LiCoO_2$/C system." *Solid State Ionics*, **1994**, *69*, 212-221.

[28]. Bruce P. G.; "Energy storage beyond the horizon: Rechargeable lithium batteries." *Solid State Ionics*, **2008**, *179*, 752-760.

[29]. Zhang Y.; Huo Q.; Duo P.; Wang L.; Zhang A.; "Advances in new cathode material LiFePO4 for Lithium-Ion s batteries" *Synthetic Metals*, **2012**, *162*, 1315-1326.

[30]. Ritchie A.; Howard W.; "Recent developments and likely advances in Lithium-ion batteries.' *J. Power Sources*, **2006**, *162*, 809-812.

[31]. Winter M.; Brodd R. J.; "What are batteries, fuel cells, and supercapacitors?" *Chem. Rev.*, **2004**, *104*, 4245-4269.

[32]. Bruce P. G.; Scrosati B.; Tarascon J. M.; "Nanomaterials for rechargeable lithium batteries." *Angew. Chem. Int. Ed.*, **2008**, *47*, 2930-2946.

[33]. Guo Y. G.; Hu J. S.; Wan, L. J.; "Nanostructured materials for electrochemical energy conversion and storage devices." *Adv. Mater.*, **2008**, *20*, 2878-2887.

[34]. Jamnik J.; Maier J.; "Nanocrystallinity effects in lithium battery materials - Aspects of nano-ionics. Part IV." *Phys. Chem. Chem. Phys.*, **2003**, *5*, 5215-5220.

[35]. Maier J.; "Nanoionics: ion transport and electrochemical storage in confined systems." *Nat. Mater.*, **2005**, *4*, 805-815.

[36]. Balaya P. "Size effects and nanostructured materials for energy applications." *Energy Environ. Sci.*, **2008**, *1*, 645-654.

[37]. Wang Q.; Li H.; Chen L. Q.; Huang X. J.; "Monodispersed hard carbon spherules with uniform nanopores." *Carbon*, **2001**, *39*, 2211-2214.

[38]. Kaskhedikar N. A.; Maier J.; "Lithium storage in carbon nanostructures." *Adv. Mater*., **2009**, *21*, 2664-2680.

[39]. Wu X. L.; Jiang L. Y.; Cao F. F.; Guo Y. G.; Wan L. J.; "$LiFePO_4$ Nanoparticles Embedded in a Nanoporous Carbon Matrix: Superior Cathode Material for Electrochemical Energy-Storage Devices." *Adv. Mater*., **2009**, *21*, 2710-2714.

[40]. Jiao F.; Bruce P. G.; "Mesoporous crystalline beta-MnO_2 a reversible positive electrode for rechargeable lithium batteries." *Adv. Mater*., **2007**, *19*, 657-660.

[41]. Balaya P.; Bhattacharyya A. J.; Jamnik J.; Zhukovskii Y. F.; Kotomin E. A.; Maier J.; "Nano-ionics in the context of lithium batteries." *J. Power Sources*, **2006**, *159*, 171-178.

[42]. Delmer O.; Balaya P.; Kienle L.; Maier J.; "Enhanced potential of amorphous electrode materials: Case study of RuO_2." *Adv. Mater*., **2008**, *20*, 501-505.

[43]. Robertson A. D.; Armstrong A. R.; Bruce P. G.; "Layered $Li_xMn_{1-y}Co_yO_2$ intercalation electrodes-influence of ion exchange on capacity and structure upon cycling." *Chem. Mater*., **2001**, *13*, 2380-2386.

[44]. Meethong N.; Huang H. Y. S.; Speakman S. A.; Carter W. C.; Chiang Y. M.; "Strain accommodation during phase transformations in olivine-based cathodes as a materials selection criterion for high-power rechargeable batteries." *Adv. Funct. Mater*., **2007**, *17*, 1115-1123.

[45]. Reimers J. N.; Dahn J. R.; "Electrochemical and in situ X-ray-diffraction studies of lithium intercalation in Li_xCoO_2." *J. Electrochem. Soc.*, **1992**, *139*, 2091-2097.

[46]. Shao-Horn Y.; Croguennec L.; Delmas C.; Nelson E. C.; O'Keefe M. A.; "Atomic resolution of Lithium-Ion s in $LiCoO_2$." *Nat. Mater.*, **2003**, *2*, 464-467.

[47]. Imanishi N.; Fujiyoshi M.; Takeda Y.; Yamamoto O.; Tabuchi M.; "Preparation and Li-7-NMR study of chemically delithiated $Li_{1-x}CoO_2$ ($0 < x < 0.5$)." *Solid State Ionics*, **1999**, *118*, 121-128.

[48]. Levasseur S.; Menetrier M.; Suard E.; Delmas C.; "Evidence for structural defects in non-stoichiometric HT-$LiCoO_2$: electrochemical, electronic properties and Li-7 NMR studies." *Solid State Ionics*, **2000**, *128*, 11-24.

[49]. Fu L. J.; Liu H.; Li C.; Wu Y. P.; Rahm E.; Holze R.; Wu H. Q.; "Surface modifications of electrode materials for Lithium-Ion batteries." *Solid State Sci.,* **2006**, *8*, 113-128.

[50]. Cao Q.; Zhang H. P.; Wang G. J.; Xia Q.; Wu Y. P.; Wu H. Q.; "A novel carbon-coated $LiCoO_2$ as cathode material for Lithium-Ion battery." *Electrochem. Commun.,* **2007**, *9*, 1228-1232.

[51]. Cho J.; Kim Y. J.; Kim,T. J.; Park,B.; "Zero-strain intercalation cathode for rechargeable Li-ion cell." *Angew. Chem. Int. Ed.,* **2001**, *40*, 3367-3369.

[52]. Cho J.; Kim Y. W.; Kim B.; Lee J. G.; Park B.; "A breakthrough in the safety of lithium secondary batteries by coating the cathode material with $AlPO_4$ nanoparticles." *Angew. Chem. Int. Ed.,* **2003**, *42*, 1618-1621.

[53]. Kim J.; Noh M.; Cho J.; Kim H.; Kim K. B.; "Controlled nanoparticle metal phosphates (metal = Al, Fe, Ce, and Sr) coatings on $LiCoO_2$ cathode materials." *J. Electrochem. Soc.,* **2005**, *152*, A1142-A1148.

[54]. Dahn J. R.; Vonsacken U.; Michal C. A.; "Structure and electrochemistry of $Li_{1+/-y}NiO_2$ and a new Li_2NiO_2 phase with the $Ni(OH)_2$ structure." *Solid State Ionics,* **1990**, *44*, 87-97.

[55]. Armstrong A. R.; Bruce P. G.; "Synthesis of layered $LiMnO_2$ as an electrode for rechargeable lithium batteries." *Nature* **1996**, *381*, 499-500.

[56]. Capitaine F.; Gravereau P.; Delmas C.; "A new variety of $LiMnO_2$ with a layered structure." *Solid State Ionics* **1996**, *89*, 197-202.

[57]. Vitins G.; West K.; "Lithium intercalation into layered $LiMnO_2$." *J. Electrochem. Soc.,* **1997**, *144*, 2587-2592.

[58]. Liu Z. L.; Yu A. S.; Lee J. Y.; "Synthesis and characterization of $LiNi_{1-x-y}Co_xMn_yO_2$ as the cathode materials of secondary lithium batteries." *J. Power Sources,* **1999**, *81*, 416-419.

[59]. Yoshio M.; Noguchi H.; Itoh J.; Okada M.; Mouri T.; "Preparation and properties of $LiCo_yMn_xNi_{1-x-y}O_2$ as a cathode for Lithium-Ion batteries." *J. Power Sources,* **2000**, *90*, 176-181.

[60]. Ohzuku T.; Makimura Y.; "Layered lithium insertion material of $LiCo_{1/3}Ni_{1/3}Mn_{1/3}O_2$ for lithium-ion batteries." *Chem. Lett.*, **2001**, *30*, 642-643.

[61]. Zhou F.; Zhao X. M.; Dahn J. R.; "Synthesis, Electrochemical Properties, and Thermal Stability of Al-Doped $LiNi_{1/3}Mn_{1/3}Co_{1/3-z}Al_zO_2$ Positive Electrode Materials." *J. Electrochem. Soc.*, **2009**, *156*, A343-A347.

[62]. Luo W. B.; Zhou F.; Zhao X. M.; Lu Z. H.; Li X. H.; Dahn J. R.; "Synthesis, Characterization, and Thermal Stability of $LiNi_{1/3}Mn_{1/3}Co_{1/3-z}Mg_zO_2$, $LiNi_{1/3-z}Mn_{1/3}Co_{1/3}Mg_zO_2$ and $LiNi_{1/3}Mn_{1/3-z}Co_{1/3}Mg_zO_2$." *Chem. Mater.*, **2010**, *22*, 1164-1172.

[63]. Zhang Y.; Huo Q.; Du P.; Wang L.; Zhang A.; Song Y.; Lv Y.; Li G.; "Advances in new cathode material $LiFePO_4$ for lithium-ion batteries." *Synthetic Metals*, **2012**, *162*, 1315-1326.

[64]. Brinker C. J.; Scherer G. W.; "Sol-Gel Science: the Physics and Chemistry of Sol-gel Processing" *Academic Press Inc.*, **1990**, New York.

[65]. Guyomard D.; Tarascon J. M.; "The carbon/$Li_{1+x}Mn_2O_4$ system." *Solid-State Ionics*, **1994**, *69*, 222-237.

[66]. Ohzuku T.; Makimura Y.; "Layered lithium insertion material of $LiCo_{1/3}Ni_{1/3}Mn_{1/3}O_2$ for lithium-ion batteries." *Chem. Lett.*, **2001**, *8*, 744-745.

[67]. Ammundsen B.; Paulsen J.; Davidson I.; Liu R. S.; Shen C. H.; Chen J. M.; Jang L. Y.; Lee J. F.; "Local Structure and First Cycle Redox Mechanism of Layered $Li_{1.2}Cr_{0.4}Mn_{0.4}O_2$ Cathode Material." *J. Electrochem. Soc.*, **2002**, *149*, A431-A434.

[68]. Karthikeyan K.; Amaresh S.; Lee G. W.; Aravindan V.; Kim H.; Kang K. S.; Kim W.S.; Lee Y. S.; "Electrochemical performance of cobalt free, $Li_{1.2}(Mn_{0.32}Ni_{0.32}Fe_{0.16})O_2$ cathodes for lithium batteries." *Electrochimica Acta*, **2012**, *68*, 246-253.

[69]. Whittingham M. S.; "Lithium Batteries and Cathode Materials" *Chem. Rev.*, **2004**, *104*, 4271-4301.

[70]. Geochemical Instrumentation and Analysis, Darrell Henry, Nelson Eby, John Goodge, David Mogk.

[71]. Geochemical Instrumentation and Analysis, Barbara L Dutrow, Louisiana State University, Christine M. Clark, Eastern Michigan University.

[72]. Geochemical Instrumentation and Analysis, Susan Swapp University of Wyoming.

[73]. Suryanarayana C.; Koch C. C.; "Nanocrystalline materials–Current research and future directions." *Hyperfine Interact*, **2000**, *130*, 5-44.

[74]. Wang Z.; Sun Y.; Chen L.; Huang X.; "Electrochemical Characterization of Positive Electrode Material $LiNi_{1/3}Co_{1/3}Mn_{1/3}O_2$ and Compatibility with Electrolyte for Lithium-Ion Batteries." *J. Electrochem. Soc.*, **2004**, *151*, A914-A921.

[75]. Luciana F. Maia.; Rodrigues Ana C. M.; "Electrical conductivity and relaxation frequency of lithium borosilicate glasses." *Solid State Ionics.*, **2004**, *168*, 87-92.

[76]. Nieto-Ramos S.; Tomer M. S.; Hernandez S.; Aliev F.; "Thin films of lithium intercalation complex oxides for cathodes." *Thin Solid Films*, **2000**, *377*, 745-749.

[77]. Tabuchi M.; Nabeshima Y.; Ado K.; Shikano M.; Kageyama H.; Tatsumi K.; "Material design concept for Fe-substituted Li< sub> 2</sub> MnO< sub> 3</sub>-based positive electrodes." J. *Power Sources*, **2007**, *174*, 554-559.

[78]. Sun Y.; Ouyang, C.; Wang Z.; Huang X.; Chen L.; "Effect of Co Content on Rate Performance of $LiMn_{0.5-x}Co_{2x}Ni_{0.5-x}O_2$ Cathode Materials for Lithium-Ion Batteries." *J. Electrochem. Soc.*, **2004**, *151*, A504-A508.

[79]. Shannon R. D.; "Revised effective ionic radii and systematic studies of interatomic distances in halides and chalcogenide." *Acta Crystallogr.*, **1976**, *32*, 751-767.

[80]. Ammundsen B.; Paulsen J.; Davidson I.; Liu R. S.; Shen C. H.; Chen J. M.; Jang L. Y.; Lee J. F.; "Local Structure and First Cycle Redox Mechanism of Layered $Li_{1.2}Cr_{0.4}Mn_{0.4}O_2$ Cathode Material." *J. Electrochem. Soc*., **2002**, *149*, A431-A436.

[81]. Ohzuku T.; Makimura Y.; "Layered lithium insertion material of $LiCo_{1/3}Ni_{1/3}Mn_{1/3}O_2$ for lithium-ion batteries." *Chem. Lett*., **2001**, *8*, 744-745.

[82]. Upadhyay R. K.; Panwar A. K. “Physico-Chemical Characterization of Cathode Material, $Li_{1+x}(Mn_{0.4}Ni_{0.4}Fe_{0.2})_{1-x}O_2$ (x=0.2) for Lithium Ion Batteries.” *International Journal of Emerging Technology and Advanced Engineering*, **2014**, *4*, 249-253.